Title

Unusual inheritance of a functional *cki* homolog in the human pathogen *Schistosoma mansoni*

Short title

Unusual inheritance of a Schistosome *cki* homolog

Authors

George R. Wendt[1], James J. Collins III[1,2]*

Affiliations

[1]Department of Pharmacology, University of Texas Southwestern Medical Center
[2]Howard Hughes Medical Institute

* To whom correspondence should be addressed

Abstract

Schistosomes, parasitic flatworms responsible for the neglected tropical disease schistosomiasis, are protected by a skin-like tegument, and tegument maintenance is controlled by a schistosome ortholog (*p53-1*) of the tumor suppressor TP53. To understand *p53-1* function, we characterized a schistosome cyclin dependent kinase inhibitor homolog (*cki*). Knockdown of *cki* resulted in hyperproliferation, that, combined with *p53-1* knockdown yielded tumor-like growths, indicating that *cki* and *p53-1* are tumor suppressors in *Schistosoma mansoni*. Interestingly, *cki* homologs are ubiquitous in parasitic flatworms but are absent from their free-living ancestors, suggesting *cki* may have come from horizontal gene transfer. This suggests that the evolution of parasitism in flatworms was aided by an unusual means of metazoan genetic inheritance.

Teaser

Horizontal gene transfer may have played an important role in the evolution of parasitic flatworms

Introduction

Parasitic flatworms are a diverse clade of organisms that include pathogens of great medical and agricultural purposes. Interestingly, all parasitic flatworms come from a single speciation event, and therefore are a derived clade relative to all free-living flatworms(*1*). As such, common traits shared across parasitic flatworms could represent early adaptations that facilitated a free-living ancestor in their transition to parasitic lifestyle. One such common trait is the presence of the tegument, a syncytial skin-like tissue that is essential for successful parasitism(*2*). Recent studies in the human pathogen *Schistosoma mansoni* have begun to elucidate the cellular and molecular mechanisms that govern tegument development(*3, 4*), including evidence that the parasite ortholog of *TP53* (*Sman-p53-1*, *p53-1* for brevity, gene symbol Smp_139530) is a master regulator of tegument development(*5*). TP53 homologs have previously been shown to regulate stem cells and epidermis production in free-living planarians(*6*), in part via its transcriptional regulation of genes essential for normal epidermis development(*7*). It is unclear how *p53-1* regulates tegument production, but one of the most well characterized mechanisms of function of TP53 homologs across a variety of animals involves its regulation of the expression of the cyclin dependent kinase inhibitors (CKIs), proteins that interact with CDK/cyclin complexes to cause cell cycle exit*(8-10)*. Direct regulation of CKIs by TP53 homologs is well established in vertebrates(*9, 11*), but the relationship between TP53 homologs and CKIs in invertebrates is less clear(*12, 13*).

Results

Having previously found that *p53-1* (Smp_139530), the schistosome homolog of TP53, plays an important role in tegument development(*5*), we sought to identify the targets of this transcription factor to understand how *p53-1* controls tegument development. We reasoned that *p53-1* and its transcriptional targets would likely have a similar expression pattern. Using our previously generated single-cell RNAseq atlas(*14*), we identified a gene (*Smp_199050*) that was expressed in many of the same cells as *p53-1*, including tegument progenitor cells and stem cells, suggesting

48 it could play a role in regulating tegument production (**Figure 1A-C**). Though this homolog did not
49 possess any close homology to any genes outside of parasitic flatworms, some of its homologs
50 in other parasitic flatworms (*e.g., Clonorchis sinensis* CSKR_104219-T1) were annotated with a
51 cyclin dependent kinase inhibitor (CDI) domain superfamily domain (InterPro entry IPR044898
52 (*15*)). Upon closer examination, Smp_199050 did bear relatively high similarity and identity to
53 other CDI-domain containing proteins such as Drosophila Dap and human CDKN1B (**Figure S1A-**
54 **B**). Additionally, the AlphaFold(*16*) predicted structure of the n-terminus of Smp_199050
55 conformed to the structure of CDKN1B when superimposed on the solved structure of
56 CDK4/CCND1/CDKN1B(*17*) (**Figure S1C**). As such, we opted to refer to Smp_199050 as *cki*
57 going forward.

58 We next tested the function of *cki* in the parasite. In other organisms, *cki* homologs act as tumor
59 suppressors in part by binding to and inhibiting the cyclin/CDK complexes that control the cell
60 cycle, halting proliferation(*18*). As such, loss of function of *cki* homologs results in
61 hyperproliferation in a variety of animals in a variety of contexts(*19-24*). When we knockdown *cki*
62 using RNAi, we similarly observe a hyperproliferation phenotype (**Figure 2, Figure S2A-B**). While
63 there is nearly 100% penetrance of the hyperproliferation phenotype in the parasite's head
64 (**Figure 2, top**), there is variable penetrance of the phenotype in the body of the worm (**Figure 2,**
65 **bottom**). This increase in proliferation appears to be accompanied by a loss of production of *tsp-*
66 *2*$^{+}$ tegument progenitor cells (**Figure 2, Figure S2A-B**) as well as new tegument cells (**Figure**
67 **S2C-D**), demonstrating that the increase in proliferation is accompanied by a loss of
68 differentiation. Additionally, we see an approximately five-fold increase in apoptotic cells in the
69 heads of *cki(RNAi)* parasites (**Figure S2E-F**). Together, this suggests that *cki* RNAi causes stem
70 cells to engage in hyperproliferation at the expense of differentiation, ultimately resulting in stem
71 cell death.

72 Human *cki* homologs are widely recognized as tumor suppressors(*18, 25*), but no studies of
73 invertebrate *cki* homologs have demonstrated spontaneous tumor formation in *cki* loss-of-function
74 models(*20-23*). Unlike most invertebrate models studied to date, schistosomes have lifespans
75 measured in decades(*26*) and rely upon proliferative somatic cells throughout these long
76 lives(*27*). As such, we wondered whether *cki* could function as a tumor suppressor in
77 schistosomes. Knockdown of *cki* alone causes hyperproliferation (**Figure 2**) but never results in
78 robust tumorigenesis. Given our original model that *cki* expression might be induced by *P53-1*
79 (**Figure 3A**), and that cki RNAi leads to hyperproliferation (**Figure 3B**), we next wondered whether
80 knocking down *p53-1* in combination with *cki* would create a more permissive environment for
81 tumor formation in the parasite (**Figure 3C**). We found that knocking down *p53-1* in conjunction
82 with *cki* does in fact result in the appearance of abnormal proliferative tumor-like masses in the
83 parasite's head with nearly 100% penetrance (**Figure 3D**). This suggests that *cki* and *p53-1*
84 cooperate as tumor suppressors in *Schistosoma mansoni*.

85 Interestingly, we were able to readily identify one or more *cki* homologs in nearly all parasitic
86 flatworm genomes (evidence of *cki* homologs present in 57 out of 60 genomes examined) (**Table**
87 **S1-2**) but were unable to find any *cki* homologs in any free-living flatworm genomes or
88 transcriptomes (present in 0 out of 37 genomes/transcriptomes examined across 10 taxonomic
89 orders) (**Figure 4A, Table S2**). Additionally, most parasitic flatworm *cki* homologs appear to sit
90 within a microsynteny block downstream of a *TIMM21* homolog and upstream of a *TUBB* homolog
91 (**Table S1**). Examination of annotated free-living flatworm genomes identified no *cki* homologs
92 downstream of their *TIMM21* homologs (**Table S3**), further supporting the absence of *cki*
93 homologs in free-living flatworms. This is surprising because phylogenetic analysis suggests that
94 all parasitic flatworms arose from a common free-living ancestor several hundred million years
95 ago(*1*). As such, any gene found broadly across parasitic clades should be present at some
96 frequency in the extant free-living flatworms. The fact that we do not observe this suggests either

97 1) the parasite *cki* homologs arose from *de novo* gene birth, 2) *cki* homologs were present broadly
98 throughout all flatworms but were independently lost in all extant free-living flatworm lineages that
99 we have transcriptomic/genomic data for, or 3) the parasite *cki* homolog was not inherited
100 "vertically" and therefore may have originated from horizontal gene transfer (HGT) in an ancestral
101 parasitic flatworm. Given that parasite *cki* homologs have sequence-level similarity to other
102 metazoan *cki* homologs (**Figure S1A-B**), de novo gene birth can be safely ruled out. While we
103 cannot rule out multiple independent losses of *cki* homologs/incomplete genomic data across
104 extant free-living flatworms, it would be incredibly unlikely that *cki* homologs were absent from 37
105 different animals across 10 taxonomic orders, leaving HGT as one of the most likely explanations
106 for the origin of parasitic flatworm *cki* based on phylogenomic analysis.

107 To further investigate the possibility of HGT, we performed phylogenetic analysis of schistosome
108 *cki* (see materials and methods for details). We first obtained a wide-reaching group of CKI
109 homologs related to the schistosome *cki* by performing an iterative DELTA-BLAST search,
110 followed by manual curation of the hits. The vast majority of CKI homologs are largely
111 unstructured except for the CDI domain located in the n-terminus (per the InterPro entry for
112 IPR003175(*15, 28*)), so we opted to specifically perform the phylogenetic maximum likelihood
113 analysis using the aligned CDI domains. This strategy was largely successful at reconstructing
114 the relationships within vertebrate CKIs (**Figure S3**): CDKN1A, CDKN1B, CDKN1C, and
115 CDKN1D homologs all clustered with themselves and each other as expected (e.g., CDKN1D is
116 most closely related to CDKN1A(*29*) than to CDKN1B/C) and maintained phylogenetic
117 relationships (Marsupial CDKN1B forms a sister clade to placental mammal CDKN1B). Most
118 invertebrate CKI homologs did not fall neatly within these clades (**Figure S3**, red asterisks), with
119 most forming a "CKI" clade that does not cluster with any of the well-characterized classes of CKI.
120 Only two exceptions to this exist: first, a small group of spiralians (*Octopus sinensis* and
121 *Helobdella robusta*) cluster together with mammalian CDKN1B (with all other mollusks and

122 annelids falling within the “CKI” clade), and second, all parasitic flatworm CKI homologs cluster
123 together with CDKN1A (**Figure 4B**, **Figure S3**, red dashed box, **Figures S4-S5**), specifically
124 within the avian clade, albeit with relatively modest support values. Together with the absence of
125 *cki* homologs in free-living flatworms, these data support HGT as a likely origin for *cki* in parasitic
126 flatworms.

127 **Discussion**

128 Tumor suppressors such as TP53 and CDKN1A are some of the most widely studied molecules
129 on the planet, but their functions in animals that do not generally develop tumors are largely
130 unexplored. Most glaringly, studies of TP53 homologs in Spiralia have been limited to a handful
131 of species of flatworms. Seminal work in planarians revealed that *Smed-p53* acts as a stem cell
132 regulator and tumor suppressor in planaria(*6*) at least in part through regulation of flatworm-
133 specific transcription factors(*7*). Our previous work demonstrated that the schistosome TP53
134 ortholog, like *Smed-p53,* acts as a stem cell regulator but, unlike *Smed-p53*, does not appear to
135 have any tumor suppressor functions(*5*), leaving open questions as to how TP53 homologs may
136 function in free-living versus parasitic flatworms. Here, we show that schistosomes have a
137 *CDKN1A* homolog, *cki*, that acts as a tumor suppressor together with the parasite’s *TP53*
138 ortholog, *p53-1*. Knocking down this *cki* homolog results in a dramatic increase in stem cell
139 proliferation with a concomitant decrease in differentiation. Knocking down *cki* in combination with
140 *p53-1* results in spontaneous and robust formation of abnormal proliferative masses of cells,
141 demonstrating that *cki* and *p53-1* are bona fide tumor suppressors in schistosomes.

142 The exact biology that underlies tumorigenesis upon knockdown of both *p53-1* and *cki* is both
143 fascinating and difficult to study. Knockdown of *cki* alone is sufficient to cause extreme levels of
144 hyperproliferation but does not appear to give rise to tumors. Knockdown of *p53-1*, on the other
145 hand, results in a depletion of proliferative cells and their progeny. Though our model is that
146 knocking down *cki* and *p53-1* at the same time results in both direct (i.e., cki RNAi) and indirect

147 (i.e., loss of *p53-1* mediated cki transcription) loss of cki transcript, enabling tumorigenesis
148 (**Figure 3A-C**), this model is difficult to directly test. *p53-1* RNAi causes a loss of the stem and
149 progenitor cells(*5*) where *cki* is expressed (**Figure 1A**), so we cannot directly test to see if
150 depletion of *p53-1* results in less *cki* transcription. Further studies of *p53-1* transcriptional targets
151 may reveal the exact nature of interaction between *cki* and *p53-1*.

152 Our findings also raise questions about the nature of tumor suppressors in flatworms. Why is loss
153 of function of TP53 orthologs sufficient to cause tumorigenesis in free-living flatworms, but
154 tumorigenesis in parasitic flatworms requires a "second hit"? The most obvious difference
155 between these animals is their ecological niche; does the parasitic lifestyle change the
156 fundamental issues that long-lived animals must tackle with respect to tumor suppression? Are
157 there other biological differences between free-living and parasitic flatworms that might be driving
158 these changes (such as the loss of piRNA in parasitic flatworms(*30*))? A comparative examination
159 of the function of "canonical" tumor suppressors in free-living and parasitic flatworms could
160 provide insights into the evolution of tumor suppressors, insights that may have implications
161 outside of the phylum Platyhelminthes. As such, future studies in this direction are of great
162 importance.

163 Perhaps most interestingly, one of the most likely origins of the parasite's *cki* homolog is horizontal
164 gene transfer. Given that parasitic flatworms all derive from a common free-living ancestor(*1*),
165 anything ubiquitous in parasitic flatworms should be present at some frequency in extant free-
166 living flatworms. That *cki* is absent from free-living flatworms led us to three unusual explanations
167 for its origin. First, we believe we can safely rule out de novo gene birth given that parasite *cki* is
168 related to other metazoan *cki* homologs on the sequence level (**Figure S1A-B**). That leaves us
169 with either 1) a situation where *cki* homologs were broadly present throughout all flatworms, but
170 then sometime after parasitic flatworms diverged over 270 million years ago(*31*), the ancestors of
171 the 10 taxonomic orders of free-living flatworms that we have genomic information for lost their

172 *cki* homologs while parasitic flatworms retained theirs or 2) a situation where an early ancestral
173 parasitic flatworm acquired a *cki* homolog via horizontal gene transfer. Even though maximum
174 likelihood analysis supports an origin for parasitic flatworm *cki* within Aves, we hesitate to
175 definitively assert that parasitic flatworm *cki* derived from any specific clade for a variety of
176 reasons. First, the support values for placement within Aves are relatively modest (UFBoot of 85
177 upon including nearest-neighbor interchange into phylogenetic analysis (**Figure S5**)). Still,
178 parasitic flatworm *cki* homologs consistently fall within CDKN1A homologs (which are only present
179 in vertebrates), supporting a vertebrate origin. Second, our method relies upon alignment of the
180 CDI domain from CKI homologs, which does exclude analysis of the unstructured regions of the
181 gene, which could contain valuable phylogenetic information, but complicate the assumptions that
182 underly most maximum likelihood analyses(*32*). Third, genomic information for invertebrates
183 (especially spiralians such as flatworms and mollusks) is relatively sparse and low quality
184 compared to the information available for vertebrates. As such, additional genomic information
185 from more spiralian organisms could change our conclusions. We attempted to compensate for
186 this by including additional spiralian *cki* sequences in our maximum likelihood analysis that did
187 not arise from our initial DELTA-BLAST search, but this does not completely eliminate the
188 limitations of spiralian genome sparsity. Finally, the donor of parasitic flatworm *cki* would have had
189 to been alive several hundred million years ago (in order to transmit its *cki* homolog to the
190 ancestral parasitic flatworm) and may not have survived the subsequent mass extinction events
191 to create modern descendants rendering attempts to identify the *cki* donor moot.

192 Further complicating the assumption that parasite *cki* came from horizontal gene transfer, HGT in
193 metazoans, especially between metazoans, is relatively rare(*33, 34*). Still, HGT in parasitic
194 flatworms might be more common than in other metazoans. HGT between multicellular organisms
195 has been frequently identified between parasitic plants and their host plants(*35-38*). Aside from
196 the analogous relationship between parasitic flatworms and their metazoan hosts, parasitic

197 flatworms may represent especially molecularly fertile ground for HGT. In addition to their syncytial
198 tegument, all parasitic flatworms are also united by their loss of the piRNA pathway(*30*) that,
199 combined with apparent the lack of DNA methylation across flatworms(*39-41*), makes the parasitic
200 flatworms deficient in two key pathways used to suppress mobile selfish genetic elements like
201 transposons and endogenous retroviruses(*33, 42, 43*). Indeed, this type of HGT has been
202 reported between parasitic lamprey and their host(*44*), both of which have intact defenses against
203 selfish genetic elements. Selfish genetic element mediated HGT could therefore be unusually
204 successful in parasitic flatworms.

205 Origin of the *cki* gene notwithstanding, the fact that it is nearly ubiquitous across all parasitic
206 flatworms means that it has been present in parasitic flatworms from early in their evolution and
207 has likely been retained because it plays an important role in these animals. Understanding that
208 role could teach us not only about the evolution of parasitism in these fascinating animals but
209 could also reveal ways to combat the diseases that they cause.

210 **Materials and Methods**

211 *Parasite acquisition and culture*

212 Adult S. mansoni (NMRI strain, 6–7 weeks post-infection) were obtained from infected female
213 mice by hepatic portal vein perfusion with 37°C DMEM (Sigma-Aldrich, St. Louis, MO) plus 10%
214 Serum (either Fetal Calf Serum or Horse Serum) and heparin. Parasites were cultured as
215 previously described(*3*). Unless otherwise noted, all experiments were performed with male
216 parasites in order to maximize the amount of somatic tissue present and to avoid additional
217 experimental modifications that have to be undertaken for successful in vitro female parasite
218 culture(*45*). Experiments with and care of vertebrate animals were performed in accordance with
219 protocols approved by the Institutional Animal Care and Use Committee (IACUC) of UT
220 Southwestern Medical Center (approval APN: 2017-102092).

221 *Labeling and imaging*

222 Schistosome colorimetric and fluorescence in situ hybridization analyses were performed as
223 previously described(*3-5, 27*) with the following modification. To improve signal-to-noise for
224 colorimetric and fluorescence in situ hybridization, worms were incubated at 95°C for 15m in
225 10mM sodium citrate, pH6.0 prior to proteinase K digestion. *in vitro* EdU labeling and detection
226 was performed as previously described(*46*). TUNEL labeling was carried out as follows:
227 formaldehyde-fixed worms stored in 100% MeOH were rehydrated in 50% MeOH/50% PBS +
228 0.3% TritonX-100 pH7.4 (PBSTx), then rinsed in PBSTx. Parasites were then photobleached as
229 described previously(*3*). After photobleaching, parasites were rinsed in PBSTx, then incubated at
230 95°C for 15m in 10mM sodium citrate pH6.0. Following this, parasites were rinsed in PBSTx then
231 permeablized in 5 µg/ml proteinase K (Ambion AM2546). Following proteinase K treatment,
232 parasites were post-fixed in 4% formaldehyde in PBSTx. Parasites were then rinsed in PBSTx
233 then incubated at 37°C in TdT reaction buffer from Click-iT™ Plus TUNEL Assay for In Situ
234 Apoptosis Detection kit (Thermo Fisher Scientific C10617) for one hour. Parasites were then
235 incubated at 37°C in TdT reaction mix for one hour per manufacturer's instructions. Parasites
236 were then thoroughly rinsed and EdU detection was carried out as previously described(*3*). All
237 fluorescently labeled parasites were counterstained with DAPI (1 µg/ml), cleared in 80% glycerol,
238 and mounted on slides with Vectashield (Vector Laboratories).

239 Confocal imaging of fluorescently labeled samples was performed on a Zeiss LSM900 Laser
240 Scanning Confocal Microscope. Unless otherwise mentioned, all fluorescence images represent
241 maximum intensity projection plots. To perform cell counts, cells were manually counted in
242 maximum intensity projection plots derived from confocal stacks. Brightfield images were acquired
243 on a Zeiss AxioZoom V16 equipped with a transmitted light base and a Zeiss AxioCam 105 Color
244 camera.

245 *RNA interference*

246 Schistosome RNAi: All RNAi experiments utilized freshly perfused male parasites between 6-7
247 weeks post-infection (separated from females). dsRNA treatments were all carried out at 30 µg/ml
248 in Basch Media 169. Double knockdown experiments were carried out at 60 µg/ml (30 µg/ml of
249 each dsRNA) for the first 4 days, then switched to 30 µg/ml (15 µg/ml of each dsRNA) for the
250 remainder of the experiment. dsRNA was generated by in vitro transcription and was replaced
251 daily for 3 days and then every other day until the end of the experiment (14 days for all
252 experiments except for EdU pulse-chase experiments, which were EdU pulsed at day 14 then
253 carried out for 8 more days). EdU pulses were performed at 5µM for 4 hours before either fixation
254 or chase as described above.

255 As a negative control for RNAi experiments, we used a non-specific dsRNA containing two
256 bacterial genes(48). cDNAs used for RNAi and in situ hybridization analyses were cloned as
257 previously described(48); oligonucleotide primer sequences are listed in **Table S4**.

258 *Phylogenetic analysis*

259 Clustal alignment of CKI sequences shown in **Figure S1A** was performed using Clustal Omega
260 Multiple Sequence Alignment(*47*) (default settings except ORDER was set to 'input')(*48, 49*) with
261 sequences corresponding to residues 14-48 of Smp_199050. Protein sequences used for
262 alignment and species abbreviations can be found in **Table S5**.

263 Domain structures of CKI homologs shown in **Figure S1B** were obtained using SMART v9.0
264 (http://smart.embl-heidelberg.de/)(*50, 51*).

265 Percent identity/similarity was determined using EMBOSS Needle PSA(*47, 52*) (default settings
266 except matrix was set to BLOSUM45) by querying Smp_199050 (*Schistosoma mansoni* CKI) vs.
267 ECG_07297 (*Echinococcus granulosus* CKI), CG1772 (*Drosophila melanogaster* Dap), or
268 CDKN1B (*Homo sapiens* CDKN1B).

269 Generation of the superimposition of schistosome *cki* on the solved structure of human
270 CDK4/CCND/CDKN1B shown in **Figure S1C** was carried out using ChimeraX(*53*) (v1.7.1 2024-
271 01-22) with the PDB entry 6p8e(*17*) and residues 1-70 of the AlphaFold(*16, 54*) prediction of
272 Smp_199050 (AF-A0A3Q0KUT0-F1-v4) using Matchmaker with default settings.

273 Identification of homologs of *Schistosoma mansoni cki* (See **Table S1**) was initially carried out
274 using Wormbase Parasite (https://parasite.wormbase.org/)(version 19.0 (March 2024))(*55, 56*).
275 Examination of *cki* (Smp_199050) homologs initially only revealed *cki* homologs in trematodes
276 (present in 27/28 unique genomes) and monogeneans (present in 1/3 unique genomes). A
277 reciprocal BLAST search of the *Hymenolepis diminuta* genome identified the *cki* homolog
278 WMSIL1_LOCUS6166 ("CDI domain-containing protein"). Wormbase Parasite then identified 12
279 additional orthologs of WMSIL1_LOCUS6166 in 12 unique cestode genomes, each of which was
280 confirmed to be a *cki* ortholog via a reciprocal BLAST search. Additional BLAST searches of
281 cestode genomes revealed 4 additional *cki* homologs (or evidence of unannotated homologs) in
282 cestodes (in total present in 16/16 unique genomes), with two being incorrectly included in the
283 gene model of TIMM21 homologs. Further examination of cestode genomes revealed that a
284 second *cki* paralog was present in all cestode genomes except for the genomes of the order
285 Diphyllobothriidea (*Dibothriocephalus latus*, *Schistocephalus solidus*, and *Spirometra*
286 *erinaceieuropaei*), so we opted to name Smp_199050 orthologs *cki-1* and cestode-specific
287 paralogs *cki-2*. Next, PlanMine v3.0 (https://planmine.mpinat.mpg.de/planmine/)(*57*) was utilized
288 to search 19 free-living flatworm transcriptomes for *cki* homologs. Further searches of
289 unannotated flatworm genomes were carried out using NCBI genome datasets
290 (https://www.ncbi.nlm.nih.gov/datasets/genome/) by searching for taxid 6157. Identification of
291 potential CKI homologs was then carried out using tblastn (default settings except matrix was set
292 to BLOSUM45) with queries of Smp_199050 (*Schistosoma mansoni* CKI), PXEA_0000526601
293 (*Protopolystoma xenopodis* CKI), and HmN_000277000 (*Hymenolepis nana* CKI). The

294 unannotated genomes searched, organism clade, genome accession number, scaffold hit from
295 the tblastn search, and e-value of each hit are listed in **Table S2**.

296 Curation and alignment of CKI protein sequences was carried out by first performing a DELTA-
297 BLAST(*58*) (version 2.12.0+) search with a query of Sman-CKI against the NCBI "nr_cluster"
298 database (downloaded on November 19th 2024) with the following parameters: -evalue 0.001 -
299 num_threads 4 -num_iterations 5 -matrix BLOSUM45 -max_target_seqs 10000 (see **Table S6**).
300 The hits from the third iteration (shaded green in **Table S6**) were then filtered by removing all non-
301 refseq(*59*) sequences (i.e., retaining only sequences with accessions beginning with "XP_" or
302 "NP_"), yielding 1381 hits from 1380 unique accessions. To ensure better representation of
303 spiralian and parasitic flatworm sequences, we also added additional refseq spiralian CKI
304 homologs (21 additional homologs, see **Table S7**) and non-refseq parasitic flatworm homologs
305 (52 additional homologs that: #1 have accessions that do not begin with "XP_", #2 have correct
306 or correctable gene models for *cki* [*Dibothriocephalus latus* CKI was excluded for this reason],
307 and #3 have unique accessions [a recent duplication in the *H. microstoma* genome results in two
308 different CKI-2 homologs with identical amino acid sequences and the same accession], see
309 **Table S1)** creating a final total of 1453 sequences. We then utilized the LAST feature (updated
310 December 22nd 2022) of MAFFT(*60, 61*) (version 7) to extract and align the CDI domains from
311 our CKI homologs using the CDI domain of human CDKN1B (residues 29-72) as the reference
312 region, with default settings except "Minimum coverage" was set to 0.3. We used. This resulted
313 in 1411 sequences (see **Table S8**), with most attrition happening to parasitic flatworm CKI
314 homologs; 36 of the 42 sequences that were lost were from parasitic flatworms. Even with this
315 attrition, we still retained 19/55 parasitic flatworm CKI homologs, which we reasoned would be
316 enough to perform robust analysis.

317 Maximum likelihood analysis and phylogenetic tree construction was carried out using IQ-
318 TREE(*62*) (IQ-TREE multicore version 2.4.0 for Linux x86 64-bit built Feb 7 2025) with the

following settings: -m TEST -bb 1000 -alrt 1000 -T AUTO --runs 10 -nm 2000 and a starting seed of 289843 for Figures 4, Figure S3 and Figure S4. The analysis in Figure S5 was carried out using IQ-TREE(*62*) (IQ-TREE multicore version 2.4.0 for Linux x86 64-bit built Feb 7 2025) with the following settings: -m TEST -bb 1000 -alrt 1000 -T AUTO --runs 10 -nm 5000 -bnni and a starting seed of 194082. ModelFinder on auto settings selected "Q.plant+I+G4" as the best-fit model. The consensus tree was then uploaded to Interactive Tree of Life(*63*) (https://itol.embl.de/) where it was manually annotated. Bootstrap values are either UFBoot(*64*) values or SH-aLRT(*65*) values as indicated in the figure legends. The unannotated consensus and maximum likelihood trees with and without nearest-neighbor interchange correction in Newick format are available in **Data S1-S4**.

Statistical analysis

Statistical analysis was carried out using one-way ANOVA tests (qPCR experiments) or two-way ANOVA with Tukey's multiple comparisons tests (all other experiments). All statistical tests were performed using GraphPad Prism v10.2.3.

References

1. C. E. Laumer, A. Hejnol, G. Giribet, Nuclear genomic signals of the 'microturbellarian' roots of platyhelminth evolutionary innovation. *eLife* **4**, (2015).
2. R. Alan Wilson, M. K. Jones, Fifty years of the schistosome tegument: discoveries, controversies, and outstanding questions. *International journal for parasitology*, (2021).
3. J. J. Collins, III, G. R. Wendt, H. Iyer, P. A. Newmark, Stem cell progeny contribute to the schistosome host-parasite interface. *eLife* **5**, (2016).
4. G. R. Wendt *et al.*, Flatworm-specific transcriptional regulators promote the specification of tegumental progenitors in *Schistosoma mansoni*. *eLife* **7**, (2018).
5. G. R. Wendt, D. A. Shiroor, C. E. Adler, J. J. Collins, 3rd, Convergent evolution of a genotoxic stress response in a parasite-specific p53 homolog. *Proceedings of the National Academy of Sciences of the United States of America* **119**, e2205201119 (2022).
6. B. J. Pearson, A. Sánchez Alvarado, A planarian p53 homolog regulates proliferation and self-renewal in adult stem cell lineages. *Development (Cambridge, England)* **137**, 213-221 (2010).
7. L. C. Cheng *et al.*, Cellular, ultrastructural and molecular analyses of epidermal cell development in the planarian Schmidtea mediterranea. *Developmental biology* **433**, 357-373 (2018).

8. K. Engeland, Cell cycle regulation: p53-p21-RB signaling. *Cell Death Differ* **29**, 946-960 (2022).
9. W. S. el-Deiry *et al.*, WAF1/CIP1 is induced in p53-mediated G1 arrest and apoptosis. *Cancer Res* **54**, 1169-1174 (1994).
10. U. Langheinrich, E. Hennen, G. Stott, G. Vacun, Zebrafish as a model organism for the identification and characterization of drugs and genes affecting p53 signaling. *Current biology : CB* **12**, 2023-2028 (2002).
11. S. Berghmans *et al.*, tp53 mutant zebrafish develop malignant peripheral nerve sheath tumors. *Proceedings of the National Academy of Sciences of the United States of America* **102**, 407-412 (2005).
12. A. K. Jolliffe, W. B. Derry, The TP53 signaling network in mammals and worms. *Briefings in Functional Genomics* **12**, 129-141 (2012).
13. W. J. Lu, J. M. Abrams, Lessons from p53 in non-mammalian models. *Cell Death Differ* **13**, 909-912 (2006).
14. G. Wendt *et al.*, A single-cell RNA-seq atlas of Schistosoma mansoni identifies a key regulator of blood feeding. *Science* **369**, 1644-1649 (2020).
15. T. Paysan-Lafosse *et al.*, InterPro in 2022. *Nucleic Acids Research* **51**, D418-D427 (2022).
16. M. Varadi *et al.*, AlphaFold Protein Structure Database in 2024: providing structure coverage for over 214 million protein sequences. *Nucleic Acids Research* **52**, D368-D375 (2023).
17. K. Z. Guiley *et al.*, p27 allosterically activates cyclin-dependent kinase 4 and antagonizes palbociclib inhibition. *Science* **366**, (2019).
18. L. Csergeová, D. Krbušek, R. Janoštiak, CIP/KIP and INK4 families as hostages of oncogenic signaling. *Cell Div* **19**, 11 (2024).
19. M. Boxem, S. van den Heuvel, lin-35 Rb and cki-1 Cip/Kip cooperate in developmental regulation of G1 progression in C. elegans. *Development (Cambridge, England)* **128**, 4349-4359 (2001).
20. S. H. Buck, D. Chiu, R. M. Saito, The cyclin-dependent kinase inhibitors, cki-1 and cki-2, act in overlapping but distinct pathways to control cell cycle quiescence during C. elegans development. *Cell Cycle* **8**, 2613-2620 (2009).
21. M. Fukuyama, S. B. Gendreau, W. B. Derry, J. H. Rothman, Essential embryonic roles of the CKI-1 cyclin-dependent kinase inhibitor in cell-cycle exit and morphogenesis in C elegans. *Developmental biology* **260**, 273-286 (2003).
22. J. C. de Nooij, M. A. Letendre, I. K. Hariharan, A cyclin-dependent kinase inhibitor, Dacapo, is necessary for timely exit from the cell cycle during Drosophila embryogenesis. *Cell* **87**, 1237-1247 (1996).
23. M. E. Lane *et al.*, Dacapo, a cyclin-dependent kinase inhibitor, stops cell proliferation during Drosophila development. *Cell* **87**, 1225-1235 (1996).
24. C. Deng, P. Zhang, J. W. Harper, S. J. Elledge, P. Leder, Mice lacking p21CIP1/WAF1 undergo normal development, but are defective in G1 checkpoint control. *Cell* **82**, 675-684 (1995).
25. A. M. Abukhdeir, B. H. Park, P21 and p27: roles in carcinogenesis and drug resistance. *Expert Rev Mol Med* **10**, e19 (2008).
26. P. F. Basch, *Schistosomes: Development, Reproduction, and Host Relations*. (Oxford University Press, New York, 1991), pp. 248.
27. J. J. Collins, III *et al.*, Adult somatic stem cells in the human parasite *Schistosoma mansoni*. *Nature* **494**, 476-479 (2013).
28. M. Blum *et al.*, The InterPro protein families and domains database: 20 years on. *Nucleic Acids Res* **49**, D344-d354 (2021).

29. R. Laranjeiro *et al.*, Cyclin-dependent kinase inhibitor p20 controls circadian cell-cycle timing. *Proceedings of the National Academy of Sciences of the United States of America* **110**, 6835-6840 (2013).
30. I. J. Tsai *et al.*, The genomes of four tapeworm species reveal adaptations to parasitism. *Nature* **496**, 57-63 (2013).
31. P. C. Dentzien-Dias *et al.*, Tapeworm eggs in a 270 million-year-old shark coprolite. *PloS one* **8**, e55007 (2013).
32. C. J. Brown, A. K. Johnson, G. W. Daughdrill, Comparing Models of Evolution for Ordered and Disordered Proteins. *Molecular Biology and Evolution* **27**, 609-621 (2009).
33. S. M. Soucy, J. Huang, J. P. Gogarten, Horizontal gene transfer: building the web of life. *Nat Rev Genet* **16**, 472-482 (2015).
34. T. Pandey *et al.*, Acquired stress resilience through bacteria-to-nematode interdomain horizontal gene transfer. *Embo j* **42**, e114835 (2023).
35. S. Yoshida, S. Maruyama, H. Nozaki, K. Shirasu, Horizontal gene transfer by the parasitic plant Striga hermonthica. *Science* **328**, 1128 (2010).
36. Z. Xi *et al.*, Horizontal transfer of expressed genes in a parasitic flowering plant. *BMC Genomics* **13**, 227 (2012).
37. Y. Zhang *et al.*, Evolution of a horizontally acquired legume gene, albumin 1, in the parasitic plant Phelipanche aegyptiaca and related species. *BMC Evol Biol* **13**, 48 (2013).
38. D. Zhang *et al.*, Root parasitic plant Orobanche aegyptiaca and shoot parasitic plant Cuscuta australis obtained Brassicaceae-specific strictosidine synthase-like genes by horizontal gene transfer. *BMC Plant Biol* **14**, 19 (2014).
39. G. Raddatz *et al.*, Dnmt2-dependent methylomes lack defined DNA methylation patterns. *Proceedings of the National Academy of Sciences of the United States of America* **110**, 8627-8631 (2013).
40. G. S. Cox, C. K. Phares, R. A. Schmidt, Molecular characterization of the Spirometra mansonoides genome: renaturation kinetics, methylation, and hybridization to human cDNA probes. *Biochimica et biophysica acta* **1049**, 134-144 (1990).
41. M. R. Fantappié, E. R. Gimba, F. D. Rumjanek, Lack of DNA methylation in Schistosoma mansoni. *Exp Parasitol* **98**, 162-166 (2001).
42. D. Li, D. H. Taylor, J. C. van Wolfswinkel, PIWI-mediated control of tissue-specific transposons is essential for somatic cell differentiation. *Cell reports* **37**, 109776 (2021).
43. J. L. Goodier, Restricting retrotransposons: a review. *Mob DNA* **7**, 16 (2016).
44. H. H. Zhang, C. Feschotte, M. J. Han, Z. Zhang, Recurrent horizontal transfers of Chapaev transposons in diverse invertebrate and vertebrate animals. *Genome Biol Evol* **6**, 1375-1386 (2014).
45. J. Wang, R. Chen, J. J. Collins, III, Systematically improved in vitro culture conditions reveal new insights into the reproductive biology of the human parasite *Schistosoma mansoni*. *PLoS biology* **17**, e3000254 (2019).
46. J. J. Collins, III, P. A. Newmark, It's no fluke: the planarian as a model for understanding schistosomes. *PLoS pathogens* **9**, e1003396 (2013).
47. F. Madeira *et al.*, Search and sequence analysis tools services from EMBL-EBI in 2022. *Nucleic acids research* **50**, W276-W279 (2022).
48. G. Yachdav *et al.*, MSAViewer: interactive JavaScript visualization of multiple sequence alignments. *Bioinformatics* **32**, 3501-3503 (2016).
49. F. Lemoine *et al.*, NGPhylogeny.fr: new generation phylogenetic services for non-specialists. *Nucleic Acids Res* **47**, W260-w265 (2019).

50. I. Letunic, P. Bork, 20 years of the SMART protein domain annotation resource. *Nucleic Acids Research* **46**, D493-D496 (2017).
51. I. Letunic, S. Khedkar, P. Bork, SMART: recent updates, new developments and status in 2020. *Nucleic Acids Res* **49**, D458-d460 (2021).
52. F. Madeira *et al.*, The EMBL-EBI Job Dispatcher sequence analysis tools framework in 2024. *Nucleic acids research* **52**, W521-W525 (2024).
53. E. C. Meng *et al.*, UCSF ChimeraX: Tools for structure building and analysis. *Protein Sci* **32**, e4792 (2023).
54. J. Jumper *et al.*, Highly accurate protein structure prediction with AlphaFold. *Nature* **596**, 583-589 (2021).
55. K. L. Howe, B. J. Bolt, M. Shafie, P. Kersey, M. Berriman, WormBase ParaSite - a comprehensive resource for helminth genomics. *Molecular and biochemical parasitology* **215**, 2-10 (2017).
56. K. L. Howe *et al.*, WormBase 2016: expanding to enable helminth genomic research. *Nucleic Acids Res* **44**, D774-780 (2016).
57. A. Rozanski *et al.*, PlanMine 3.0-improvements to a mineable resource of flatworm biology and biodiversity. *Nucleic Acids Res* **47**, D812-d820 (2019).
58. G. M. Boratyn *et al.*, Domain enhanced lookup time accelerated BLAST. *Biology Direct* **7**, 12 (2012).
59. T. Goldfarb *et al.*, NCBI RefSeq: reference sequence standards through 25 years of curation and annotation. *Nucleic Acids Research* **53**, D243-D257 (2024).
60. K. Katoh, J. Rozewicki, K. D. Yamada, MAFFT online service: multiple sequence alignment, interactive sequence choice and visualization. *Briefings in Bioinformatics* **20**, 1160-1166 (2017).
61. S. Kuraku, C. M. Zmasek, O. Nishimura, K. Katoh, aLeaves facilitates on-demand exploration of metazoan gene family trees on MAFFT sequence alignment server with enhanced interactivity. *Nucleic Acids Research* **41**, W22-W28 (2013).
62. B. Q. Minh *et al.*, IQ-TREE 2: New Models and Efficient Methods for Phylogenetic Inference in the Genomic Era. *Molecular Biology and Evolution* **37**, 1530-1534 (2020).
63. I. Letunic, P. Bork, Interactive Tree of Life (iTOL) v6: recent updates to the phylogenetic tree display and annotation tool. *Nucleic Acids Research*, (2024).
64. B. Q. Minh, M. A. T. Nguyen, A. von Haeseler, Ultrafast Approximation for Phylogenetic Bootstrap. *Molecular Biology and Evolution* **30**, 1188-1195 (2013).
65. S. Guindon *et al.*, New algorithms and methods to estimate maximum-likelihood phylogenies: assessing the performance of PhyML 3.0. *Syst Biol* **59**, 307-321 (2010).

Acknowledgments

Non-author contributions: Schistosome infected mice and *B. glabrata* snails were provided by the National Institute of Allergy and Infectious Diseases Schistosomiasis Resource Center of the Biomedical Research Institute (Rockville, MD, USA) through National Institutes of Health National Institute of Allergy and Infectious Diseases Contract HHSN272201700014I for distribution through BEI Resources.

Funding:

National Institutes of Health grant R01AI121037 (JJC)

National Institutes of Health grant R01AI167967 (JJC)

National Institutes of Health grant R01AI150776 (JJC)

Welch Foundation I-1948-20240404 (JJC)

Howard Hughes Medical Institute (JJC).

Author Contributions:

Conceptualization: GRW, JJC

Methodology: GRW, JJC

Investigation: GRW, JJC

Supervision: JJC

Writing—original draft: GRW, JJC

Writing—review & editing: GRW, JJC

Competing interests: Authors declare that they have no competing interests.

Data and materials availability: All data are available in the main text or the supplementary materials.

Supplementary materials:

Fig. S1-5

Tables S1-8

Data S1-4

Figures and Tables

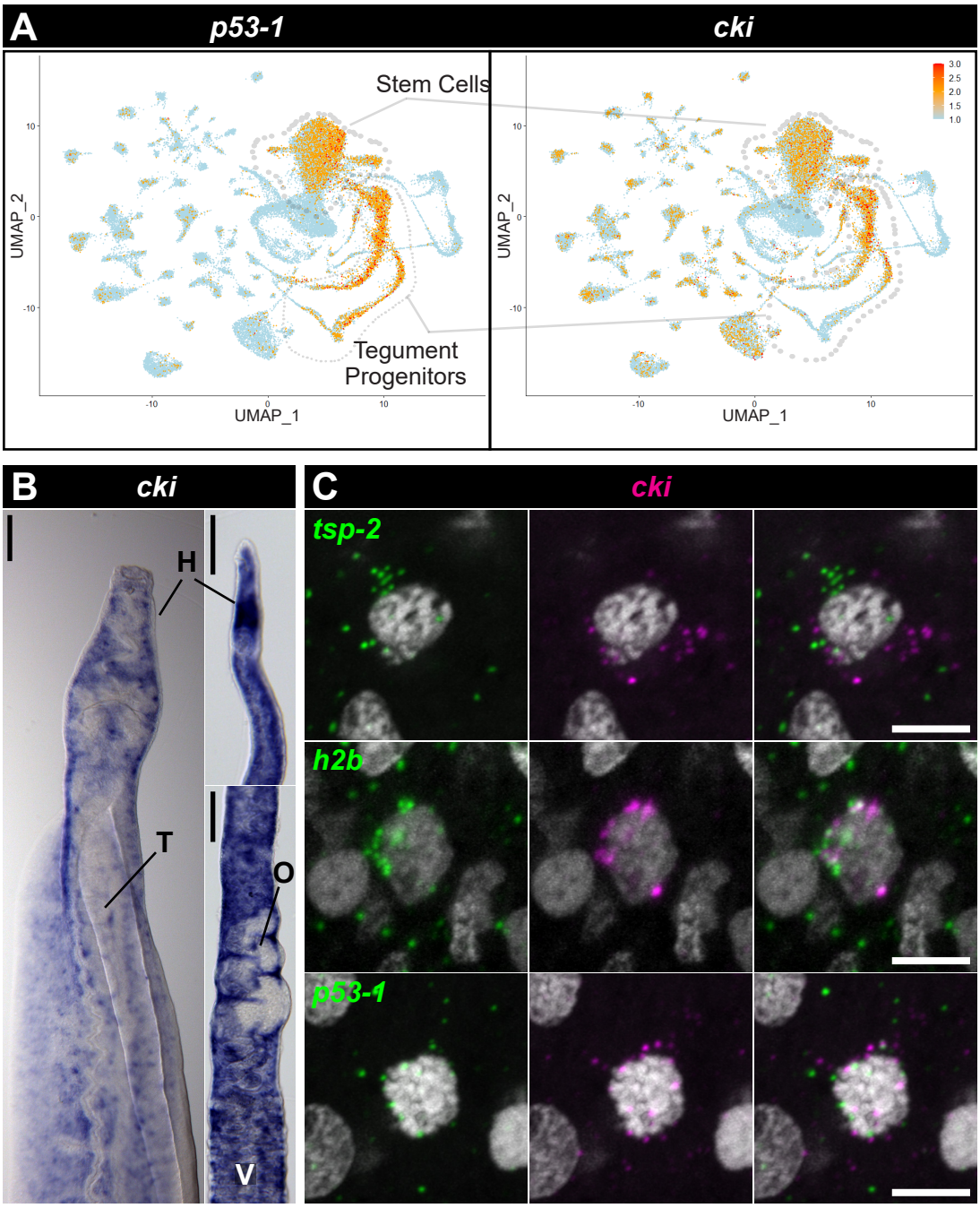
A
p53-1
cki
Stem Cells
Tegument Progenitors
UMAP_2
UMAP_1
B
cki
H
T
O
V
C
cki
tsp-2
h2b
p53-1

507 **Fig. 1. *cki* is co-expressed with the schistosome homolog of *TP53*.** A) Uniform manifold
508 approximation plots showing expression patterns of *p53-1* and *cki* in adult schistosomes. Red
509 indicates high expression, orange indicates medium expression, and blue indicates low/no
510 expression. B) Colorimetric WISH showing expression patterns of *cki* in male (left) and female
511 (right) worms. H, head; T, testes; O, ovary; V, vitellaria. C) Double FISH experiment showing
512 expression of *cki* relative to the tegument progenitor marker *tsp-2*, the proliferative cell marker
513 *h2b*, and *p53-1*. Scale bars: (B) 500 μm, (C) 5 μm.

514

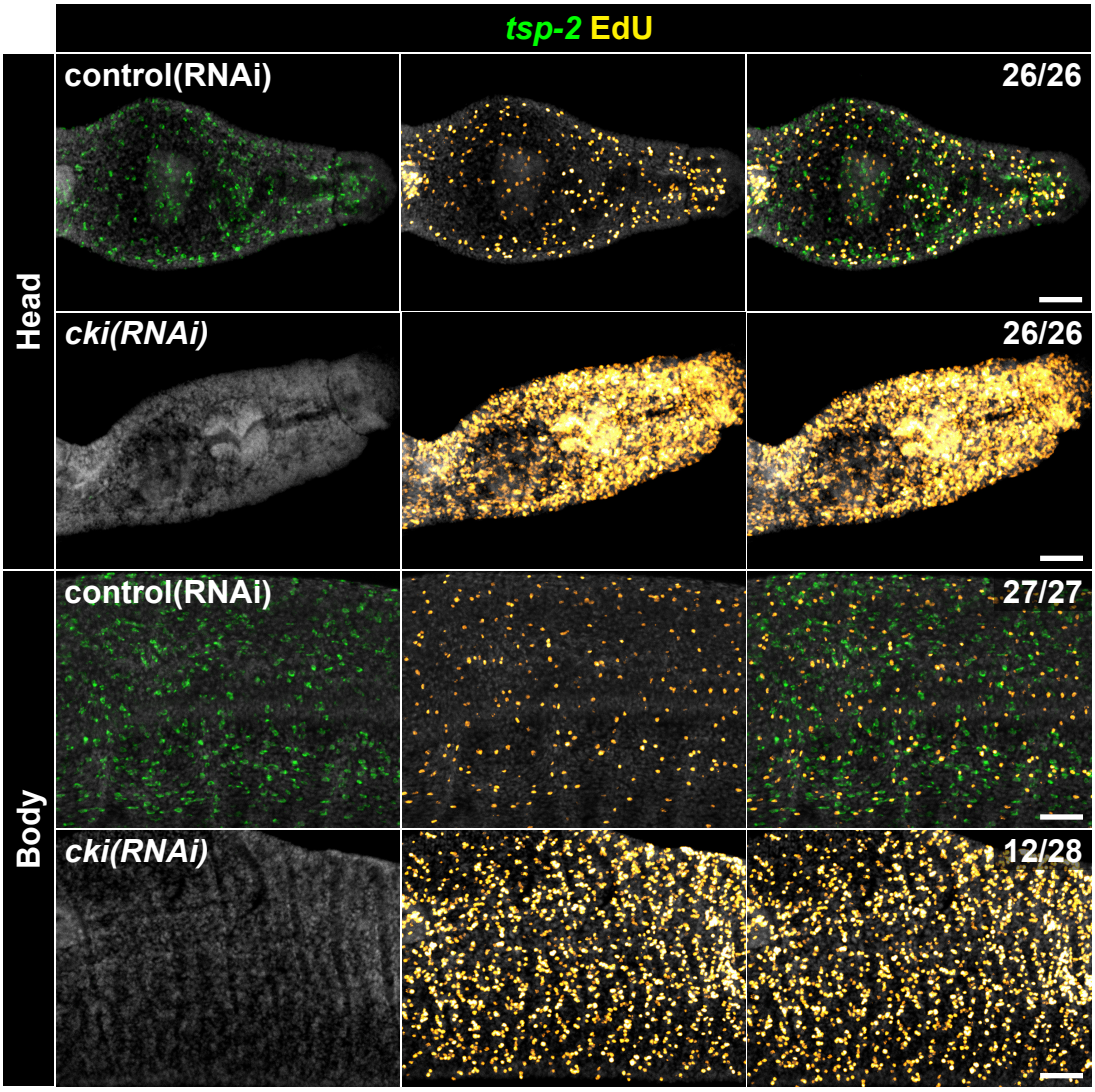
tsp-2 EdU
Head
control(RNAi)
26/26
cki(RNAi)
26/26
Body
control(RNAi)
27/27
cki(RNAi)
12/28

515 **Fig. 2. *cki* RNAi results in an increase in proliferation at the expense of differentiation.**
516 Representative images of FISH experiment in conjunction with EdU detection showing expression
517 pattern of the tegument progenitor marker *tsp-2* (green) in conjunction with the presence of
518 proliferative EdU^+ cells (yellow) under the indicated RNAi conditions. The fraction indicates the
519 number of worms that are similar to the representative image. Data are from >26
520 parasites/treatment from three biological replicates. Scale bar: 50 μm.

521

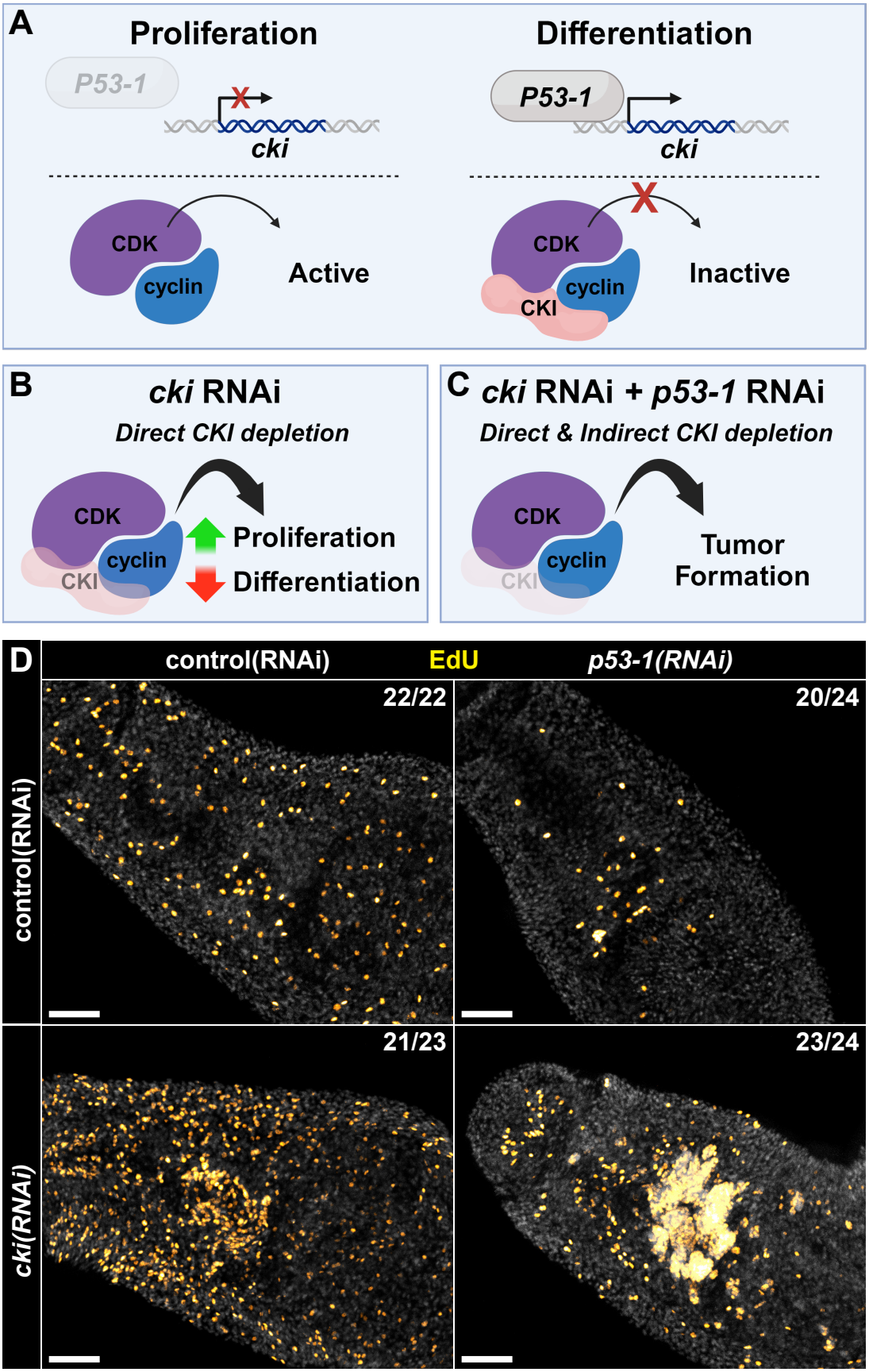
A
Proliferation
Differentiation
P53-1
cki
P53-1
cki
CDK
cyclin
Active
CDK
cyclin
CKI
Inactive
B
cki RNAi
Direct CKI depletion
CDK
cyclin
CKI
Proliferation
Differentiation
C
cki RNAi + p53-1 RNAi
Direct & Indirect CKI depletion
CDK
cyclin
CKI
Tumor
Formation
D
control(RNAi)
EdU
p53-1(RNAi)
control(RNAi)
cki(RNAi)
22/22
20/24
21/23
23/24

522 **Fig. 3. *cki* and *p53-1* cooperate as tumor suppressors in *Schistosoma mansoni*.** (A) Cartoon
523 depicting model of *p53-1* and *cki* interaction in normal parasites. In proliferative cells, P53-1
524 activity is low and *cki* is not transcribed, resulting in active cyclin/CDK complexes, promoting
525 proliferation. When proliferative cells commit to differentiating, P53-1 activity is high and *cki* is
526 transcribed, resulting in inactive cyclin/CDK/CKI complexes, promoting differentiation. (B) Cartoon
527 depicting consequences of *cki* RNAi. By knocking down *cki*, cyclin/CDK complexes are
528 inappropriately active, leading to increased proliferation and decreased differentiation. (C)
529 Cartoon depicting model of knocking down *cki* and *p53-1* simultaneously. Knocking down *cki*
530 directly depletes CKI protein. Knocking down *p53-1* may decrease P53-1-dependent induction of
531 *cki* expression. This combination may lower CKI levels low enough that proliferating cells become
532 abnormal and form tumors. (D) Representative image of EdU labelled proliferative cells in
533 parasites treated with control RNAi, *p53-1* RNAi, *cki* RNAi, or a combination of *p53-1* and *cki*
534 RNAi. Data are from >22 parasites/treatment from 3 three biological replicates. The fraction
535 indicates the number of worms that are similar to the representative image. Scale bar: 50 μm.

536

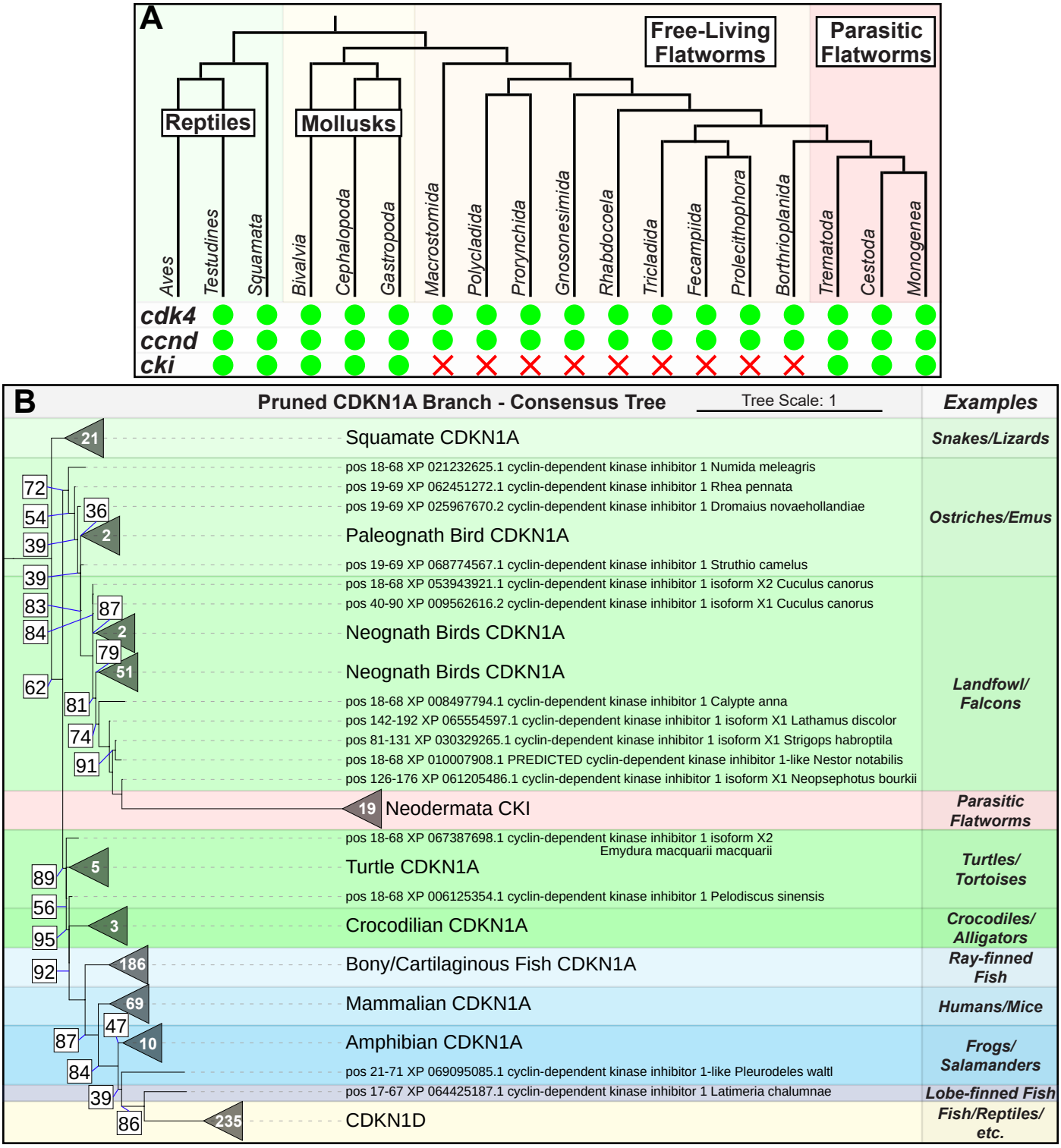
A
Free-Living Flatworms
Parasitic Flatworms
Reptiles
Mollusks
Aves
Testudines
Squamata
Bivalvia
Cephalopoda
Gastropoda
Macrostomida
Polycladida
Prorynchida
Gnosonesimida
Rhabdocoela
Tricladida
Fecampiida
Prolecithophora
Borthrioplanida
Trematoda
Cestoda
Monogenea
cdk4
ccnd
cki
B
Pruned CDKN1A Branch - Consensus Tree
Tree Scale: 1
Examples
Squamate CDKN1A
Snakes/Lizards
pos 18-68 XP 021232625.1 cyclin-dependent kinase inhibitor 1 Numida meleagris
pos 19-69 XP 062451272.1 cyclin-dependent kinase inhibitor 1 Rhea pennata
pos 19-69 XP 025967670.2 cyclin-dependent kinase inhibitor 1 Dromaius novaehollandiae
Paleognath Bird CDKN1A
pos 19-69 XP 068774567.1 cyclin-dependent kinase inhibitor 1 Struthio camelus
Ostriches/Emus
pos 18-68 XP 053943921.1 cyclin-dependent kinase inhibitor 1 isoform X2 Cuculus canorus
pos 40-90 XP 009562616.2 cyclin-dependent kinase inhibitor 1 isoform X1 Cuculus canorus
Neognath Birds CDKN1A
Neognath Birds CDKN1A
pos 18-68 XP 008497794.1 cyclin-dependent kinase inhibitor 1 Calypte anna
pos 142-192 XP 065554597.1 cyclin-dependent kinase inhibitor 1 isoform X1 Lathamus discolor
pos 81-131 XP 030329265.1 cyclin-dependent kinase inhibitor 1 isoform X1 Strigops habroptila
pos 18-68 XP 010007908.1 PREDICTED cyclin-dependent kinase inhibitor 1-like Nestor notabilis
pos 126-176 XP 061205486.1 cyclin-dependent kinase inhibitor 1 isoform X1 Neopsephotus bourkii
Landfowl/ Falcons
Neodermata CKI
Parasitic Flatworms
pos 18-68 XP 067387698.1 cyclin-dependent kinase inhibitor 1 isoform X2
Emydura macquarii macquarii
Turtle CDKN1A
pos 18-68 XP 006125354.1 cyclin-dependent kinase inhibitor 1 Pelodiscus sinensis
Turtles/ Tortoises
Crocodilian CDKN1A
Crocodiles/ Alligators
Bony/Cartilaginous Fish CDKN1A
Ray-finned Fish
Mammalian CDKN1A
Humans/Mice
Amphibian CDKN1A
pos 21-71 XP 069095085.1 cyclin-dependent kinase inhibitor 1-like Pleurodeles waltl
Frogs/ Salamanders
pos 17-67 XP 064425187.1 cyclin-dependent kinase inhibitor 1 Latimeria chalumnae
Lobe-finned Fish
CDKN1D
Fish/Reptiles/ etc.

537 **Fig. 4. Phylogenetic analysis of parasitic flatworm CKI suggests a horizontal transfer from**
538 **a distantly related metazoan.** (A) Top. Cladogram of select metazoans showing the relationship
539 between vertebrates (reptiles) and different invertebrates (mollusks, free-living flatworms, and
540 parasitic flatworms). Bottom. Chart indicating the presence or absence of *cdk4*, *ccnd*, and *cki*
541 homologs in the above species. Green circles indicate presence and red x's indicate absence.
542 (B) Pruned phylogenetic tree (617 members) showing the clade of CDKN1A homologs from the
543 phylogenetic analysis of *S. mansoni* CKI. All parasitic flatworm CKI molecules sit within the avian
544 clade. The white number inside each collapsed branch (triangle) indicates how many members
545 there are in each branch. The number in the white box indicates the UFBoot bootstrap
546 approximation value. Support values for branches with UFBoot support greater than 95 are not
547 shown. Data are from 10 runs.

548

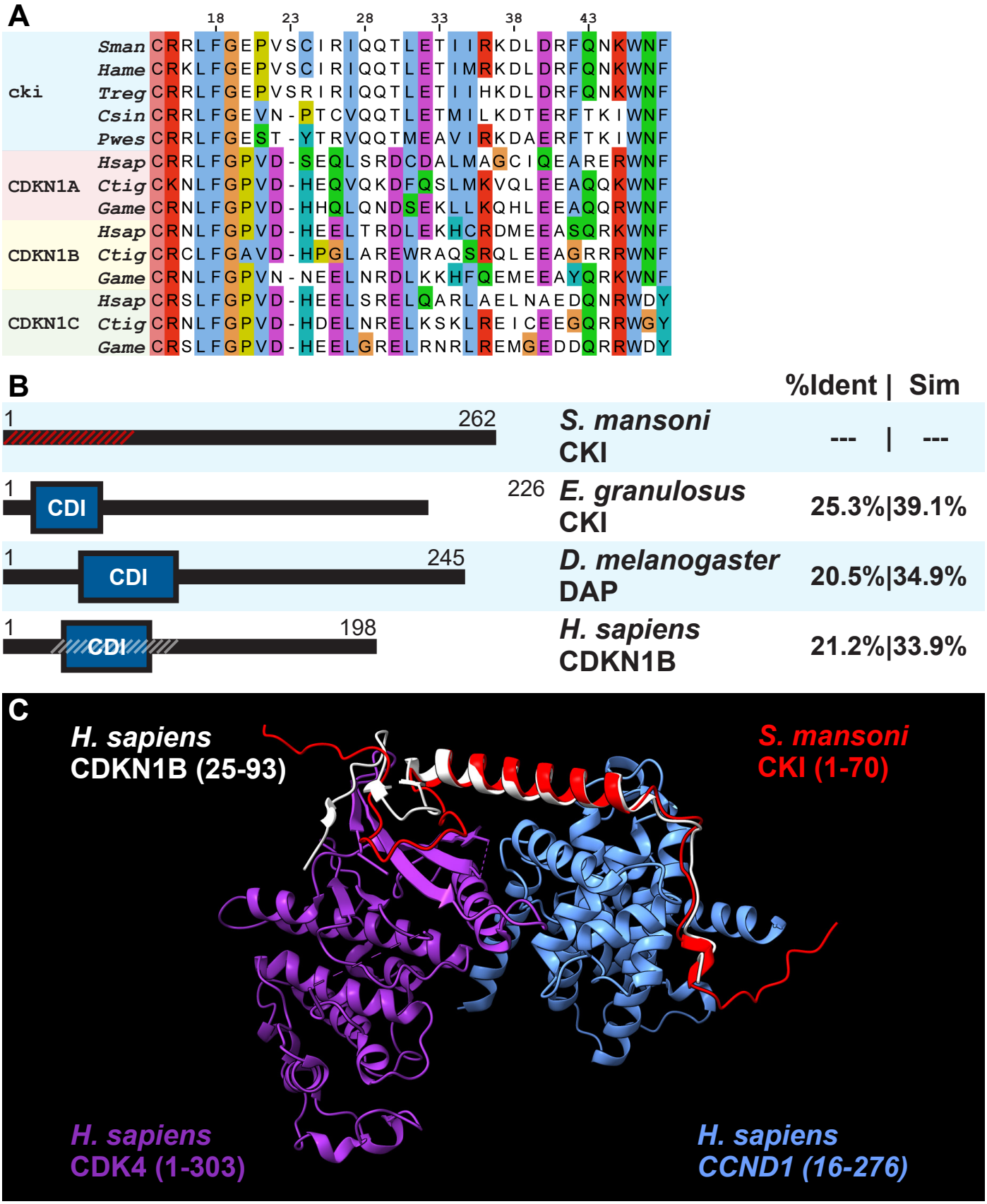
A
18 23 28 33 38 43
cki
Sman CRRLFGEPVSCIRIQQTLETIIRKDLDRFQNKWNF
Hame CRKLFGEPVSCIRIQQTLETIMRKDLDRFQNKWNF
Treg CRRLFGEPVSRIRIQQTLETIIHKDLDRFQNKWNF
Csin CRRLFGEVN-PTCVQQTLETMILKDTERFTKIWNF
Pwes CRRLFGEST-YTRVQQTMEAVIRKDAERFTKIWNF
CDKN1A
Hsap CRRLFGPVD-SEQLSRDCDALMAGCIQEARERWNF
Ctig CKNLFGPVD-HEQVQKDFQSLMKVQLEEAQQKWNF
Game CRNLFGPVD-HHQLQNDSEKLLKQHLEEAQQRWNF
CDKN1B
Hsap CRNLFGPVD-HEELTRDLEKHCRDMEEASQRKWNF
Ctig CRCLFGAVD-HPGLAREWRAQSRQLEEAGRRRWNF
Game CRNLFGPVN-NEELNRDLKKHFQEMEEAYQRKWNF
CDKN1C
Hsap CRSLFGPVD-HEELSRELQARLAELNAEDQNRWDY
Ctig CRNLFGPVD-HDELNRELKSKLREICEEGQRRWGY
Game CRSLFGPVD-HEELGRELRNRLREMGEDDQRRWDY
B
%Ident | Sim
1 262
S. mansoni CKI
--- | ---
1 CDI 226
E. granulosus CKI
25.3%|39.1%
1 CDI 245
D. melanogaster DAP
20.5%|34.9%
1 CDI 198
H. sapiens CDKN1B
21.2%|33.9%
C
H. sapiens CDKN1B (25-93)
S. mansoni CKI (1-70)
H. sapiens CDK4 (1-303)
H. sapiens CCND1 (16-276)

Fig. S1.

Figure S1. *Schistosoma mansoni* CKI protein domains/structure. (A) Clustal alignment of *Schistosoma mansoni* (*Sman*) CKI (Smp_199050) residues 14-48 with CKI sequences from a variety of parasitic flatworms (*Heterobilharzia americana – Hame*, *Trichobilharzia regenti – Treg*, *Clonorchis sinensis – Csin*, *Paragonimus westermani – Pwes*) as well as CDKN1A, CDKN1B, and CDKN1C sequences from humans (*Hsap*), tiger rattlesnakes (*Ctig*), and whooping cranes (*Game*). The number at top of alignment corresponds to position in the alignment relative to the *Schistosoma mansoni* CKI. Protein sequences used for alignment can be found in **Table S5** (B) Schematic of the domain structure of CKI homologs from *S. mansoni*, *E. granulosus*, *D. melanogaster*, and *H. sapiens* along with the percentage identity/similarity relative to the *S. mansoni* CKI homolog. (C) Superimposition of the AlphaFold indicated residues of *S. mansoni* CKI (accession: AF_A0A3Q0KUT0-F1-model_v4) onto the solved structure of *H. sapiens* CDKN1B, CCND1, and CDK4 (PDB accession: 6p8e). Hash-shaded portion from (B) corresponds to the superimposition in (C).

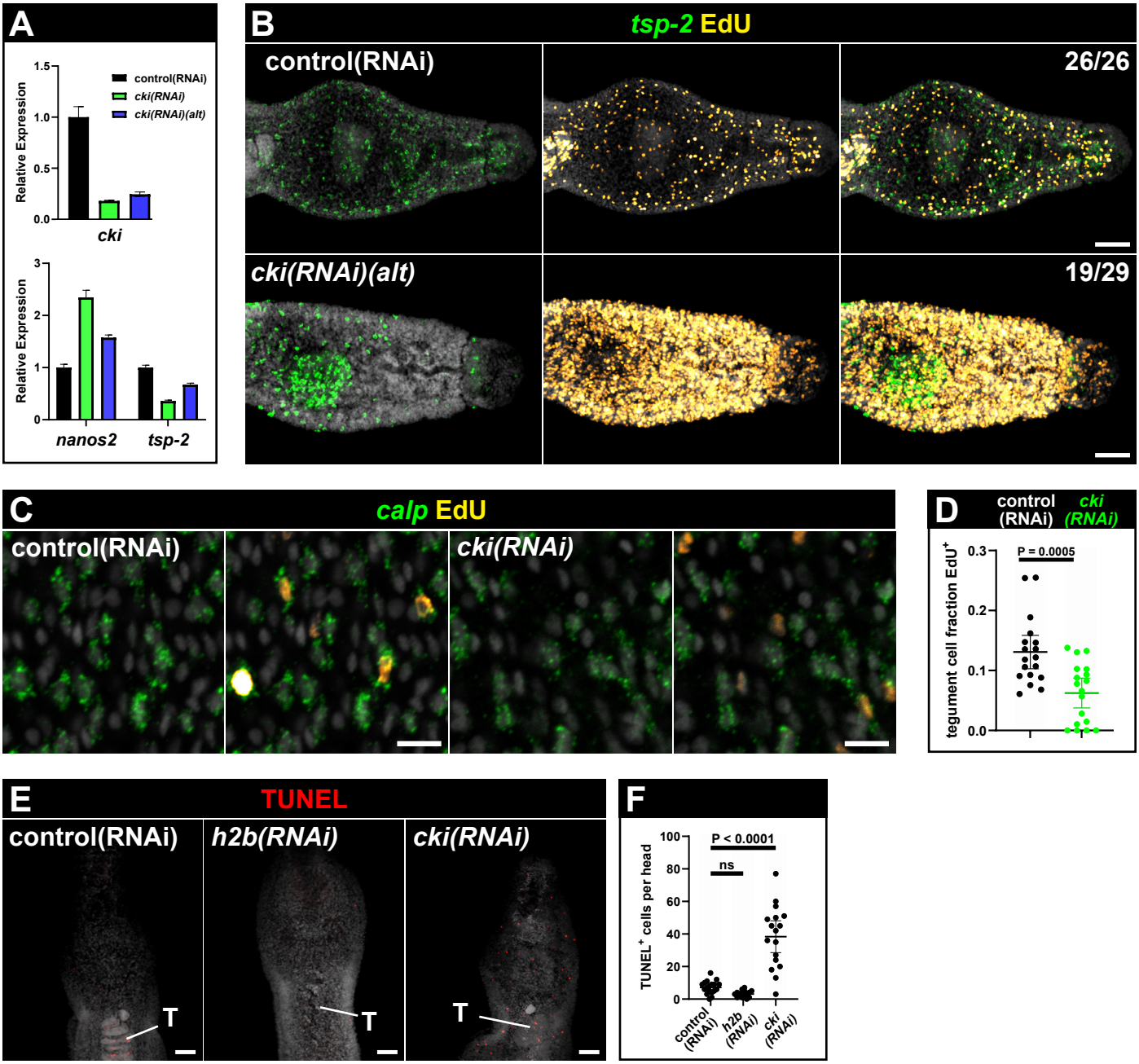
A
Relative Expression
control(RNAi)
cki(RNAi)
cki(RNAi)(alt)
cki
nanos2
tsp-2
B
tsp-2 EdU
control(RNAi)
26/26
cki(RNAi)(alt)
19/29
C
calp EdU
control(RNAi)
cki(RNAi)
D
control (RNAi)
cki (RNAi)
P = 0.0005
tegument cell fraction EdU+
E
TUNEL
control(RNAi)
h2b(RNAi)
cki(RNAi)
T
F
P < 0.0001
ns
TUNEL+ cells per head
control (RNAi)
h2b (RNAi)
cki (RNAi)

Fig. S2.

Figure S2. *cki* RNAi results in an increase in proliferation at the expense of differentiation. (A) qPCR showing expression of *cki*, the stem cell marker *nanos2*, and the tegument progenitor marker *tsp-2* under indicated RNAi conditions. 'cki(RNAi)(alt)' indicates knockdown performed with dsRNA corresponding to a non-overlapping sequence relative to the original dsRNA sequence. Data are from one biological replicate. (B) FlSH experiment in conjunction with EdU detection showing expression pattern of the tegument progenitor marker *tsp-2* (green) in conjunction with the presence of proliferative EdU^+ cells (yellow) under the indicated RNAi conditions. Note that the micrographs for control(RNAi) are duplicates of the micrographs for control(RNAi) from Figure 3 (top) as these came from the same experiment. Data are from >26 parasites/treatment from three biological replicates. (C) EdU pulse-chase experiment combined with FISH of the tegument marker *calp* after control or *cki* RNAi. Neoblast progeny are labeled with EdU after an 8-day chase. (D) Quantification of (C). Data are from 18 parasites/treatment from two biological replicates. (E) Fluorescent TUNEL assay labeling DNA breaks in worms under the indicated RNAi conditions. T, testes. Scale bar: 50 µm. Note signal in the testes is a normal occurrence in the parasite's germline. (F) Quantification of (E). Data are from >16 parasites/treatment from three biological replicates. Scale bars: (B) 50 µm, (C) 10 µm. (E) 50 µm.

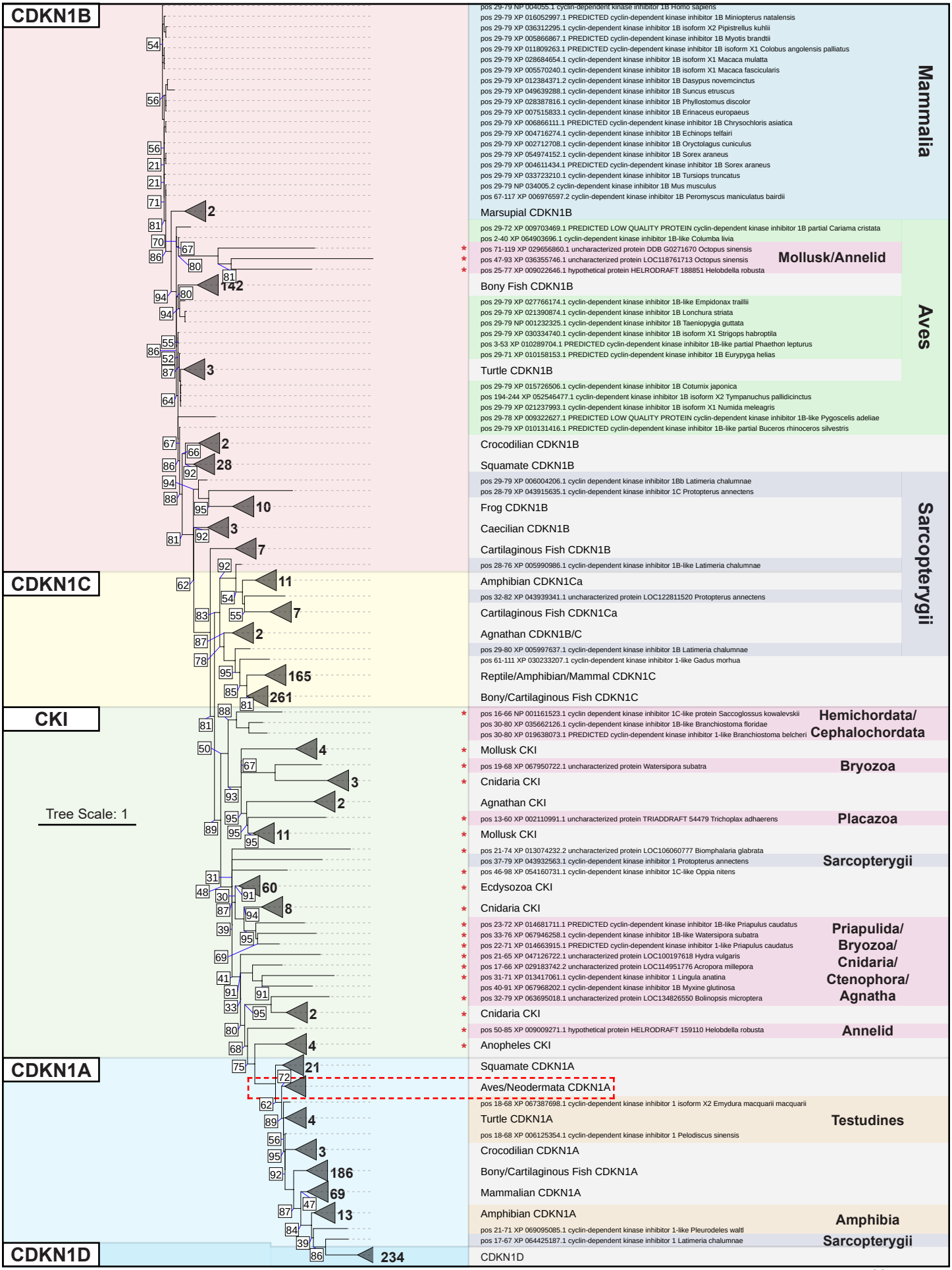
CDKN1B
CDKN1C
CKI
CDKN1A
CDKN1D
Tree Scale: 1
pos 29-79 NP 004055.1 cyclin-dependent kinase inhibitor 1B Homo sapiens
pos 29-79 XP 016052997.1 PREDICTED cyclin-dependent kinase inhibitor 1B Miniopterus natalensis
pos 29-79 XP 036312295.1 cyclin-dependent kinase inhibitor 1B isoform X2 Pipistrellus kuhlii
pos 29-79 XP 005866867.1 PREDICTED cyclin-dependent kinase inhibitor 1B Myotis brandtii
pos 29-79 XP 011809263.1 PREDICTED cyclin-dependent kinase inhibitor 1B isoform X1 Colobus angolensis palliatus
pos 29-79 XP 028684654.1 cyclin-dependent kinase inhibitor 1B isoform X1 Macaca mulatta
pos 29-79 XP 005570240.1 cyclin-dependent kinase inhibitor 1B isoform X1 Macaca fascicularis
pos 29-79 XP 012384371.2 cyclin-dependent kinase inhibitor 1B Dasypus novemcinctus
pos 29-79 XP 049639288.1 cyclin-dependent kinase inhibitor 1B Suncus etruscus
pos 29-79 XP 028387816.1 cyclin-dependent kinase inhibitor 1B Phyllostomus discolor
pos 29-79 XP 007515833.1 cyclin-dependent kinase inhibitor 1B Erinaceus europaeus
pos 29-79 XP 006866111.1 PREDICTED cyclin-dependent kinase inhibitor 1B Chrysochloris asiatica
pos 29-79 XP 004716274.1 cyclin-dependent kinase inhibitor 1B Echinops telfairi
pos 29-79 XP 002712708.1 cyclin-dependent kinase inhibitor 1B Oryctolagus cuniculus
pos 29-79 XP 054974152.1 cyclin-dependent kinase inhibitor 1B Sorex araneus
pos 29-79 XP 004611434.1 PREDICTED cyclin-dependent kinase inhibitor 1B Sorex araneus
pos 29-79 XP 033723210.1 cyclin-dependent kinase inhibitor 1B Tursiops truncatus
pos 29-79 NP 034005.2 cyclin-dependent kinase inhibitor 1B Mus musculus
pos 67-117 XP 006976597.2 cyclin-dependent kinase inhibitor 1B Peromyscus maniculatus bairdii
Marsupial CDKN1B
Mammalia
pos 29-72 XP 009703469.1 PREDICTED LOW QUALITY PROTEIN cyclin-dependent kinase inhibitor 1B partial Cariama cristata
pos 2-40 XP 064903696.1 cyclin-dependent kinase inhibitor 1B-like Columba livia
pos 71-119 XP 029656860.1 uncharacterized protein DDB G0271670 Octopus sinensis
pos 47-93 XP 036355746.1 uncharacterized protein LOC118761713 Octopus sinensis
pos 25-77 XP 009022646.1 hypothetical protein HELRODRAFT 188851 Helobdella robusta
Mollusk/Annelid
Bony Fish CDKN1B
pos 29-79 XP 027766174.1 cyclin-dependent kinase inhibitor 1B-like Empidonax traillii
pos 29-79 XP 021390874.1 cyclin-dependent kinase inhibitor 1B Lonchura striata
pos 29-79 NP 001232325.1 cyclin-dependent kinase inhibitor 1B Taeniopygia guttata
pos 29-79 XP 030334740.1 cyclin-dependent kinase inhibitor 1B isoform X1 Strigops habroptila
pos 3-53 XP 010289704.1 PREDICTED cyclin-dependent kinase inhibitor 1B-like partial Phaethon lepturus
pos 29-71 XP 010158153.1 PREDICTED cyclin-dependent kinase inhibitor 1B Eurypyga helias
Aves
Turtle CDKN1B
pos 29-79 XP 015726506.1 cyclin-dependent kinase inhibitor 1B Coturnix japonica
pos 194-244 XP 052546477.1 cyclin-dependent kinase inhibitor 1B isoform X2 Tympanuchus pallidicinctus
pos 29-79 XP 021237993.1 cyclin-dependent kinase inhibitor 1B isoform X1 Numida meleagris
pos 29-78 XP 009322627.1 PREDICTED LOW QUALITY PROTEIN cyclin-dependent kinase inhibitor 1B-like Pygoscelis adeliae
pos 29-79 XP 010131416.1 PREDICTED cyclin-dependent kinase inhibitor 1B-like partial Buceros rhinoceros silvestris
Crocodilian CDKN1B
Squamate CDKN1B
pos 29-79 XP 006004206.1 cyclin dependent kinase inhibitor 1Bb Latimeria chalumnae
pos 28-79 XP 043915635.1 cyclin-dependent kinase inhibitor 1C Protopterus annectens
Frog CDKN1B
Caecilian CDKN1B
Cartilaginous Fish CDKN1B
pos 28-76 XP 005990986.1 cyclin-dependent kinase inhibitor 1B-like Latimeria chalumnae
Sarcopterygii
Amphibian CDKN1Ca
pos 32-82 XP 043939341.1 uncharacterized protein LOC122811520 Protopterus annectens
Cartilaginous Fish CDKN1Ca
Agnathan CDKN1B/C
pos 29-80 XP 005997637.1 cyclin-dependent kinase inhibitor 1B Latimeria chalumnae
pos 61-111 XP 030233207.1 cyclin-dependent kinase inhibitor 1-like Gadus morhua
Reptile/Amphibian/Mammal CDKN1C
Bony/Cartilaginous Fish CDKN1C
pos 16-66 NP 001161523.1 cyclin dependent kinase inhibitor 1C-like protein Saccoglossus kowalevskii
pos 30-80 XP 035662126.1 cyclin-dependent kinase inhibitor 1B-like Branchiostoma floridae
pos 30-80 XP 019638073.1 PREDICTED cyclin-dependent kinase inhibitor 1-like Branchiostoma belcheri
Hemichordata/ Cephalochordata
Mollusk CKI
pos 19-68 XP 067950722.1 uncharacterized protein Watersipora subatra
Bryozoa
Cnidaria CKI
Agnathan CKI
pos 13-60 XP 002110991.1 uncharacterized protein TRIADDRAFT 54479 Trichoplax adhaerens
Placazoa
Mollusk CKI
pos 21-74 XP 013074232.2 uncharacterized protein LOC106060777 Biomphalaria glabrata
pos 37-79 XP 043932563.1 cyclin-dependent kinase inhibitor 1 Protopterus annectens
Sarcopterygii
pos 46-98 XP 054160731.1 cyclin-dependent kinase inhibitor 1C-like Oppia nitens
Ecdysozoa CKI
Cnidaria CKI
pos 23-72 XP 014681711.1 PREDICTED cyclin-dependent kinase inhibitor 1B-like Priapulus caudatus
pos 33-76 XP 067946258.1 cyclin-dependent kinase inhibitor 1B-like Watersipora subatra
pos 22-71 XP 014663915.1 PREDICTED cyclin-dependent kinase inhibitor 1-like Priapulus caudatus
pos 21-65 XP 047126722.1 uncharacterized protein LOC100197618 Hydra vulgaris
pos 17-66 XP 029183742.2 uncharacterized protein LOC114951776 Acropora millepora
pos 31-71 XP 013417061.1 cyclin-dependent kinase inhibitor 1 Lingula anatina
pos 40-91 XP 067968202.1 cyclin-dependent kinase inhibitor 1B Myxine glutinosa
pos 32-79 XP 063695018.1 uncharacterized protein LOC134826550 Bolinopsis microptera
Priapulida/ Bryozoa/ Cnidaria/ Ctenophora/ Agnatha
Cnidaria CKI
pos 50-85 XP 009009271.1 hypothetical protein HELRODRAFT 159110 Helobdella robusta
Annelid
Anopheles CKI
Squamate CDKN1A
Aves/Neodermata CDKN1A
pos 18-68 XP 067387698.1 cyclin-dependent kinase inhibitor 1 isoform X2 Emydura macquarii macquarii
Turtle CDKN1A
pos 18-68 XP 006125354.1 cyclin-dependent kinase inhibitor 1 Pelodiscus sinensis
Testudines
Crocodilian CDKN1A
Bony/Cartilaginous Fish CDKN1A
Mammalian CDKN1A
Amphibian CDKN1A
pos 21-71 XP 069095085.1 cyclin-dependent kinase inhibitor 1-like Pleurodeles waltl
Amphibia
pos 17-67 XP 064425187.1 cyclin-dependent kinase inhibitor 1 Latimeria chalumnae
Sarcopterygii
CDKN1D

Fig. S3.

Figure S3. Phylogenetic analysis of parasitic flatworm CKI suggests a horizontal transfer from a distantly related metazoan. Full consensus tree (1411 members) from maximum likelihood analysis of *S. mansoni* CKI. Left: CKI homologs generally fall into CDKN1A (blue), CDKN1B (red), CDKN1C (yellow), and CDKN1D groupings (dark blue). Homologs that did not cluster neatly within any of these groups are grouped together as "CKI" (green). The number next to each collapsed branch indicates how many members are in each branch. Right: Individual homologs are labeled with aligned residues, RefSeq accession, gene name, and species name. When possible, individual homologs were grouped together and labeled accordingly (e.g., "Bony Fish CDKN1B"). When clades did not group together into one or two clusters, they were instead labeled with colored shading (e.g., "Aves" in green shading). Invertebrate CKI molecules are labeled with red asterisks. The clade that contains avian CDKN1A along with parasitic flatworm CKI is indicated with a dashed red box. The black number next to each collapsed branch (triangle) indicates how many members there are in each branch. The number in the white box indicates the UFBoot bootstrap approximation value. Support values for branches with UFBoot support greater than 95 are not shown. Data are from 10 runs.

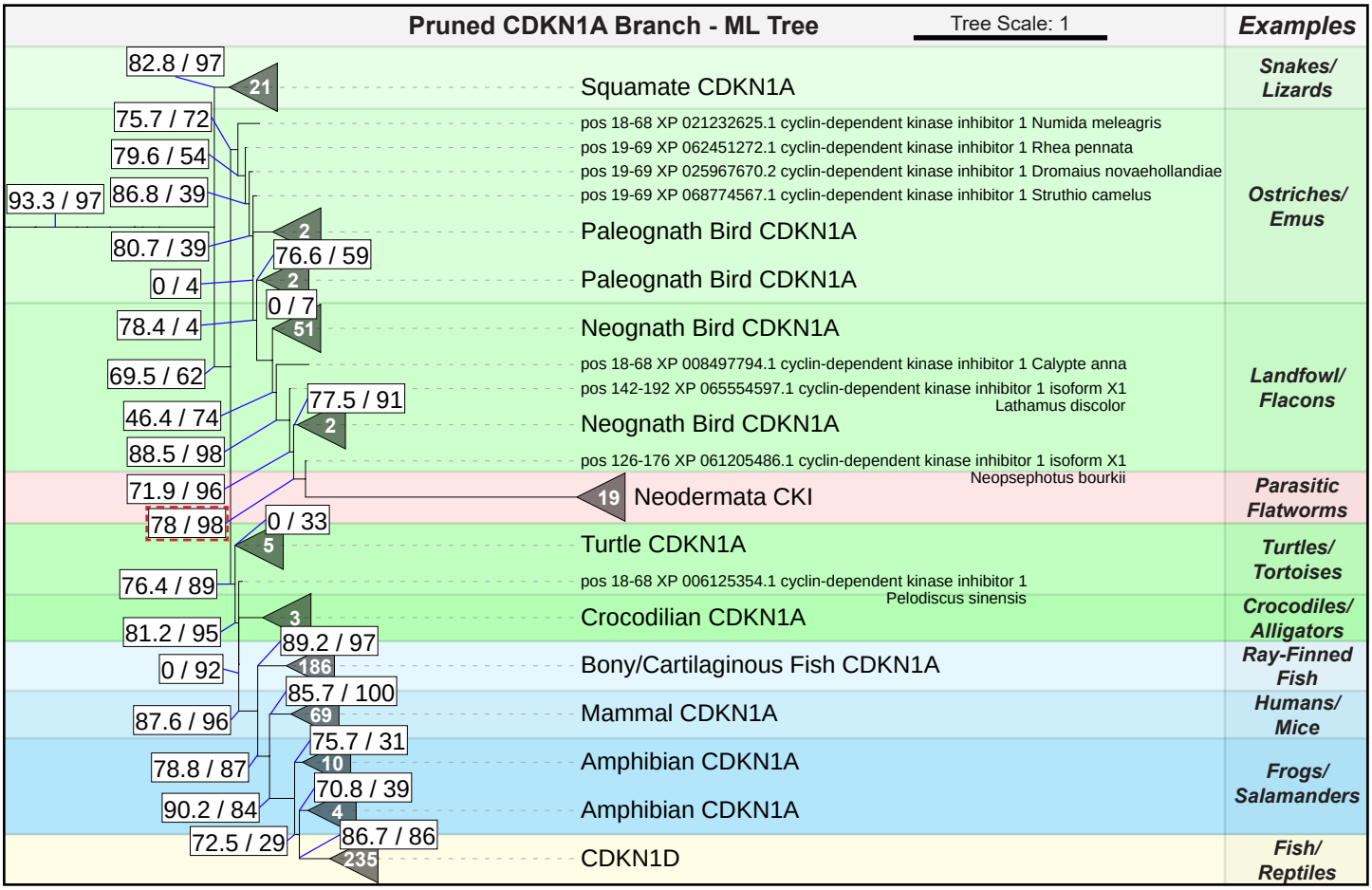
Pruned CDKN1A Branch - ML Tree
Tree Scale: 1
Examples
82.8 / 97
21
Squamate CDKN1A
Snakes/ Lizards
75.7 / 72
79.6 / 54
93.3 / 97
86.8 / 39
pos 18-68 XP 021232625.1 cyclin-dependent kinase inhibitor 1 Numida meleagris
pos 19-69 XP 062451272.1 cyclin-dependent kinase inhibitor 1 Rhea pennata
pos 19-69 XP 025967670.2 cyclin-dependent kinase inhibitor 1 Dromaius novaehollandiae
pos 19-69 XP 068774567.1 cyclin-dependent kinase inhibitor 1 Struthio camelus
Ostriches/ Emus
80.7 / 39
2
Paleognath Bird CDKN1A
76.6 / 59
0 / 4
2
Paleognath Bird CDKN1A
0 / 7
78.4 / 4
51
Neognath Bird CDKN1A
69.5 / 62
pos 18-68 XP 008497794.1 cyclin-dependent kinase inhibitor 1 Calypte anna
77.5 / 91
pos 142-192 XP 065554597.1 cyclin-dependent kinase inhibitor 1 isoform X1
Lathamus discolor
46.4 / 74
2
Neognath Bird CDKN1A
88.5 / 98
pos 126-176 XP 061205486.1 cyclin-dependent kinase inhibitor 1 isoform X1
Neopsephotus bourkii
Landfowl/ Flacons
71.9 / 96
19
Neodermata CKI
Parasitic Flatworms
78 / 98
0 / 33
5
Turtle CDKN1A
Turtles/ Tortoises
76.4 / 89
pos 18-68 XP 006125354.1 cyclin-dependent kinase inhibitor 1
Pelodiscus sinensis
3
Crocodilian CDKN1A
Crocodiles/ Alligators
81.2 / 95
89.2 / 97
0 / 92
186
Bony/Cartilaginous Fish CDKN1A
Ray-Finned Fish
85.7 / 100
87.6 / 96
69
Mammal CDKN1A
Humans/ Mice
75.7 / 31
78.8 / 87
10
Amphibian CDKN1A
70.8 / 39
90.2 / 84
4
Amphibian CDKN1A
Frogs/ Salamanders
72.5 / 29
86.7 / 86
235
CDKN1D
Fish/ Reptiles

Fig. S4.

Phylogeny of CKI within CDKN1A – Maximum Likelihood Tree. Pruned maximum likelihood phylogenetic tree (617 members) showing the clade of CDKN1A homologs from the phylogenetic analysis of *S. mansoni* CKI. The white number inside each collapsed branch (triangle) indicates how many members there are in each branch. The number in the white box indicates the Shimodaira–Hasegawa approximate Likelihood Ratio Test (SH-aLRT) value (left) and the UFBoot bootstrap approximation value (right). Support values for branches with SH-aLRT support greater than 95 are not shown. Data are from 10 runs.

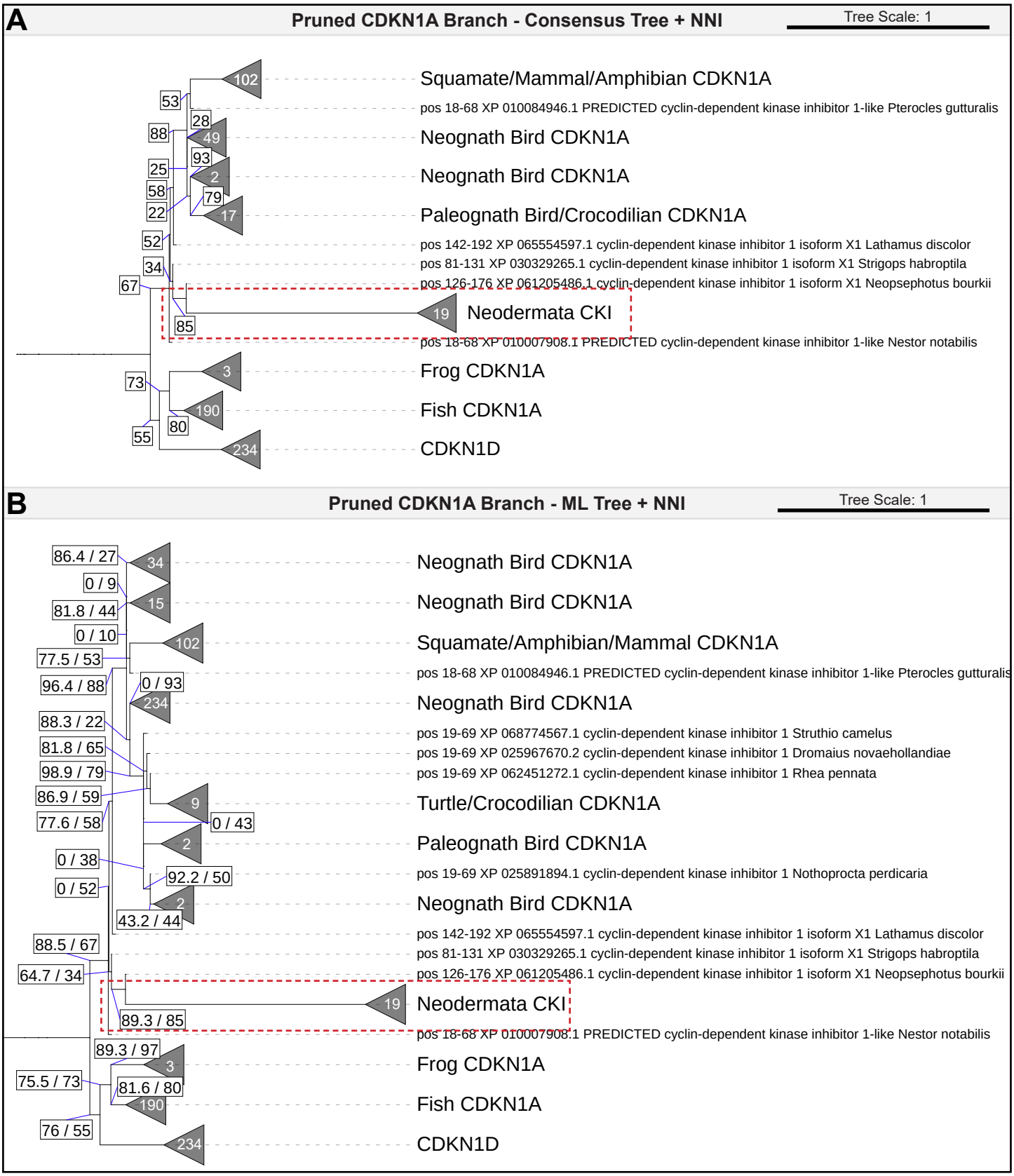
A
Pruned CDKN1A Branch - Consensus Tree + NNI
Tree Scale: 1
102
53
28
88
49
93
25
2
58
79
22
17
52
34
67
85
19
73
3
190
80
55
234
Squamate/Mammal/Amphibian CDKN1A
pos 18-68 XP 010084946.1 PREDICTED cyclin-dependent kinase inhibitor 1-like Pterocles gutturalis
Neognath Bird CDKN1A
Neognath Bird CDKN1A
Paleognath Bird/Crocodilian CDKN1A
pos 142-192 XP 065554597.1 cyclin-dependent kinase inhibitor 1 isoform X1 Lathamus discolor
pos 81-131 XP 030329265.1 cyclin-dependent kinase inhibitor 1 isoform X1 Strigops habroptila
pos 126-176 XP 061205486.1 cyclin-dependent kinase inhibitor 1 isoform X1 Neopsephotus bourkii
Neodermata CKI
pos 18-68 XP 010007908.1 PREDICTED cyclin-dependent kinase inhibitor 1-like Nestor notabilis
Frog CDKN1A
Fish CDKN1A
CDKN1D
B
Pruned CDKN1A Branch - ML Tree + NNI
Tree Scale: 1
86.4 / 27
34
0 / 9
81.8 / 44
15
0 / 10
102
77.5 / 53
96.4 / 88
0 / 93
234
88.3 / 22
81.8 / 65
98.9 / 79
86.9 / 59
9
77.6 / 58
0 / 43
2
0 / 38
92.2 / 50
0 / 52
2
43.2 / 44
88.5 / 67
64.7 / 34
19
89.3 / 85
89.3 / 97
3
75.5 / 73
81.6 / 80
190
76 / 55
234
Neognath Bird CDKN1A
Neognath Bird CDKN1A
Squamate/Amphibian/Mammal CDKN1A
pos 18-68 XP 010084946.1 PREDICTED cyclin-dependent kinase inhibitor 1-like Pterocles gutturalis
Neognath Bird CDKN1A
pos 19-69 XP 068774567.1 cyclin-dependent kinase inhibitor 1 Struthio camelus
pos 19-69 XP 025967670.2 cyclin-dependent kinase inhibitor 1 Dromaius novaehollandiae
pos 19-69 XP 062451272.1 cyclin-dependent kinase inhibitor 1 Rhea pennata
Turtle/Crocodilian CDKN1A
Paleognath Bird CDKN1A
pos 19-69 XP 025891894.1 cyclin-dependent kinase inhibitor 1 Nothoprocta perdicaria
Neognath Bird CDKN1A
pos 142-192 XP 065554597.1 cyclin-dependent kinase inhibitor 1 isoform X1 Lathamus discolor
pos 81-131 XP 030329265.1 cyclin-dependent kinase inhibitor 1 isoform X1 Strigops habroptila
pos 126-176 XP 061205486.1 cyclin-dependent kinase inhibitor 1 isoform X1 Neopsephotus bourkii
Neodermata CKI
pos 18-68 XP 010007908.1 PREDICTED cyclin-dependent kinase inhibitor 1-like Nestor notabilis
Frog CDKN1A
Fish CDKN1A
CDKN1D

Fig. S5.

Phylogeny of CKI within CDKN1A – With Nearest Neighbor Interchange. Pruned (621 members) (A) consensus or (B) maximum likelihood phylogenetic tree (generated using nearest neighbor interchange to correct for model violations) showing the clade of CDKN1A homologs from the phylogenetic analysis of *S. mansoni* CKI. The dashed red box indicates that branchpoint between avian CDKN1A and parasitic flatworm CKI. The white number inside each collapsed branch (triangle) indicates how many members there are in each branch. In (A), the number in the white box indicates the UFBoot bootstrap approximation value. Support values for branches with UFBoot support greater than 95 are not shown. In (B), the number in the white box indicates the Shimodaira–Hasegawa approximate Likelihood Ratio Test value (left) and the UFBoot bootstrap approximation value (right). Support values for branches with SH-aLRT support and UFBoot support greater than 95 are not shown. Data are from 10 runs.

Table S1. (separate file)

List of parasitic flatworm *CKI* homologs including the source organism, gene accession number(s), genomic location, amino acid sequence, upstream/downstream genes, and miscellaneous notes.

Table S2. (separate file)

List of flatworms available on NCBI that are at time of writing unannotated. Organism name, clade, and genome assembly are indicated. This table also contains the results of a tblastn search using S. mansoni, P. xenopodis, or H. microstoma CKI as a query against the indicated genome reported as the scaffold and e value of the hit.

Table S3. (separate file)

List of free-living flatworm TIMM21 homologs and the genes located downstream of these homologs.

Table S4. (separate file)

List of oligonucleotides used to produce riboprobes/dsRNA as well as primers used to perform qPCR.

Table S5. (separate file)

Accession numbers, organisms, and sequences used to generate the multiple sequence alignment in Fig S1A.

Table S6. (separate file)

Results of the DELTA-BLAST search performed as described in materials and methods. Iteration 3 (used for downstream analysis) is shaded green.

Table S7. (separate file)

FASTA format of the sequences of addtional CKI homologs from spiralians that did not appear in the initial DELTA-BLAST search.

Table S8. (separate file)

Output of the MAFFT-LAST algorithm used as described in the materials and methods.

Data S1. (separate file)

Newick format consensus tree of data shown in Fig. 4B and Fig. S3

Data S2. (separate file)
Newick format maximum likelihood tree of data shown in Fig. S4

Data S3. (separate file)
Newick format consensus tree of data shown in Fig. 5A

Data S4. (separate file)
Newick format maximum likelihood tree of data shown in Fig. 5B